

Search for a heavy neutral Higgs boson in a left-right model with an inverse seesaw mechanism at the LHC

M. Ashry^{1,3,a}, K. Ezzat^{2,3,b} and S. Khalil^{3,c}

¹*Department of Mathematics, Faculty of Science, Cairo University, Giza 12613, Egypt.*

²*Department of Mathematics, Faculty of Science, Ain Shams University, Cairo 11566, Egypt.*

³*Center for Fundamental Physics, Zewail City of Science and Technology, 6th of October City, Giza 12578, Egypt.*

(Dated: July 12, 2021)

We develop a low scale left-right symmetric model based on $SU(3)_C \times SU(2)_L \times SU(2)_R \times U(1)_{B-L} \times Z_2$ with a simplified Higgs sector consisting of only one bidoublet and one $SU(2)_R$ doublet. In this model, the tiny values of light neutrino masses are generated through an inverse-seesaw mechanism. We emphasize that in this setup, the tree-level flavor changing neutral current can be strongly suppressed, consistent with the current experimental constraints. We show that the lightest CP -even Higgs boson, which is like the standard model Higgs boson, and the next lightest Higgs boson, h' , are generated from the neutral components of the bidoublet. We show that the mass of the next lightest Higgs boson can be of an order a few hundred GeVs. We analyze the detection of h' at the Large Hadron Collider (LHC) for a center-of-mass energy $\sqrt{s} = 14$ TeV and integrated luminosity $L_{\text{int}} = 300 \text{ fb}^{-1}$ via di-Higgs channel: $h' \rightarrow hh \rightarrow b\bar{b}\gamma\gamma$ and also in the ZZ channel: $h' \rightarrow ZZ \rightarrow 4\ell$ ($\ell = e, \mu$) at an integrated luminosity $L_{\text{int}} = 3000 \text{ fb}^{-1}$. We consider three benchmark points for this analysis with $m_{h'} = 250$ GeV, 400 GeV, and 600 GeV. We show that promising signals with good statistical significances can be obtained in di-Higgs channel, with $2\gamma + 2b$ -jets final states.

I. INTRODUCTION

The Standard Model (SM) of particle physics is in an excellent agreement with most of the confirmed experimental results. However, there exist several compelling arguments that indicate that the SM is only an effective low energy limit of a more fundamental underlying theory. Indeed, there are a number of theoretical and phenomenological outstanding issues in particle physics that can not be explained and the SM fails to address them adequately. Here, we may just mention the puzzles of dark matter and tiny neutrino masses [1–5], which can not be explained within the SM. One of the most popular extensions of the SM is the grand unified theory (GUT), where the SM gauge symmetry $SU(3)_C \times SU(2)_L \times U(1)_Y$ is extended to a bigger (simple or semisimple) group. Nonvanishing neutrino masses motivate the existence of right-handed neutrinos, and hence, all known fermions would have both left and right chirality. In this respect, the SM gauge group would be extended to the left-right (LR) symmetric gauge group, which is based on $SU(3)_C \times SU(2)_L \times SU(2)_R \times U(1)_{B-L}$, where left and right chirality are treated equally at high energy scales. In this class of models, the Majorana right-handed neutrinos are naturally heavy, and hence small left-handed neutrino masses are generated through seesaw mechanisms.

In the conventional LR model proposed by Mohapatra *et al.* [6–8], the SM fermions (including the right-handed neutrino) are assigned in left- or right-handed doublets, and the following Higgs sector has been assumed: one bidoublet to construct the Yukawa couplings of quarks and leptons, in addition to a left- and right-handed scalar triplets for seesaw neutrino masses. The $SU(2)_R \times U(1)_{B-L}$ symmetry is broken down to $U(1)_Y$, at a high energy scale, by the vacuum expectation value (VEV) of the neutral component of the right-handed triplet, while the VEVs of neutral components of the bidoublet and the left-handed triplet contribute in breaking the electroweak symmetry, $SU(2)_L \times U(1)_Y$, down to $U(1)_{\text{em}}$. It was clear that the Higgs sector of this model is not minimal, with several neutral and singly and doubly charged components. Also, the left-handed triplet was introduced only to preserve LR

^a mustafa@sci.cu.edu.eg

^b kareemezzat@sci.asu.edu.eg

^c skhalil@zewailcity.edu.eg

symmetry, although its VEV must be fine-tuned to a very small value to avoid stringent constraints from the observed neutrino masses. Moreover, the Higgs triplets may induce tree level flavor violating processes that contradict the current experimental limits. Therefore, different variants of the conventional LR model have been considered [9–14].

Here, we consider an example of a LR model, with a Higgs sector consisting of one scalar bidoublet and a scalar right-handed doublet. In this case and in order to generate light neutrino masses, we adopt the inverse-seesaw (IS) mechanism [15–19]. As known, this mechanism requires introducing other singlet fermions that couple with right-handed neutrinos and have a small mass [$\sim \mathcal{O}(1)$ KeV], which may be generated radiatively. The IS mechanism is quite motivated by having the TeV scale LR model that can be probed in current and future colliders, while in the conventional LR model, the GUT scale is the typical scale of breaking LR symmetry, where right-handed neutrino masses are generated. Moreover, in the limit of vanishing the above mentioned tiny mass, we will have massless left-handed neutrinos and the lepton number symmetry is restored. Thus, such a small scale can be considered, according to 't Hooft naturalness criteria [20], as a natural scale of a global symmetry (lepton number) breaking. We also argue that in this class of models the tree-level flavor changing neutral current (FCNC) is under control. It turns out that the right-handed doublet is essentially decoupled from the two Higgs doublets, generated from the bidoublet; hence the Higgs sector of this model mimics the scenario of two the Higgs doublet model [21–23]. We show that the lightest CP -even Higgs boson, the SM-like Higgs boson, and the next lightest are generated from the neutral components of the bidoublet. For a wide range of the parameter space, one can show that the mass of the next lightest Higgs boson is of the order a few hundred GeVs.

In this paper we analyze the discovery prospects of the next lightest CP -even neutral Higgs boson, h' , at the Large Hadron Collider (LHC). Our searches are performed by looking for resonant peaks in two processes, namely $h' \rightarrow hh \rightarrow b\bar{b}\gamma\gamma$ and $h' \rightarrow ZZ \rightarrow 4\ell$ ($\ell = e, \mu$). The analysis is pivoted on three benchmark points, with $m_{h'} = 250$ GeV, 400 GeV, and 600 GeV, for a center-of-mass energy $\sqrt{s} = 14$ TeV and $L_{\text{int}} = 300 \text{ fb}^{-1}$, and 3000 fb^{-1} , respectively. After imposing various sets of cuts to reduce backgrounds (B) and improve the statistical significance (S/\sqrt{B}), where S refers to the signal, we find that the SM-like Higgs boson pair production, with $b\bar{b}\gamma\gamma$ final states, is the most promising channel for probing our heavy Higgs boson at the LHC. The channel of the Z -pair production, decay to 4ℓ is less significant as its cross section is very small for $m_{h'} \gtrsim 300$ GeV, and the associated background is quite large for $m_{h'} \simeq 200$ GeV. We show that to probe h' through this channel, L_{int} must be increased up to $L_{\text{int}} = 3000 \text{ fb}^{-1}$.

The paper is organized as follows. In Sec. II we introduce the LR model with IS mechanism. The Higgs sector of this model is discussed in Sec. III. We show that the SM-like Higgs, h , and the next lightest h' are stemmed from the real part of neutral components of the bidoublet. Searches for h' at the LHC are comprehensively studied in Sec. IV. A detailed analysis for the SM Higgs pair production from h' , followed by the decays into $b\bar{b}\gamma\gamma$, is provided. We show that the total cross section of this process is of order $\mathcal{O}(1)$ fb. In general the signal of this channel is much smaller than the background, however by selecting an appropriate set of cuts we can probe the signal with a reasonable significance. We also analyze a possible signature through the Z -gauge boson pair production from h' followed by the decays to 4ℓ . Our conclusions and final remarks are given in Sec. V.

II. LEFT-RIGHT MODEL WITH INVERSE SEESAW (LRIS)

In this section we introduce a minimal left-right model with an inverse-seesaw (LRIS), which is based on gauge symmetry $SU(3)_C \times SU(2)_L \times SU(2)_R \times U(1)_{B-L}$. The fermion content of this model is as the same as its counterpart in the conventional left-right models [6–13]. In addition, three SM singlet fermions S_1 with $B-L$ charge $= +2$ and three singlet fermions S_2 with $B-L$ charge $= -2$ are considered to implement the IS mechanism for neutrino masses. Note that we introduce pair of singlet fermions $S_{1,2}$ with opposite $B-L$ charges to keep the $U(1)_{B-L}$ anomaly free. The Higgs sector of the LRIS model consists of an $SU(2)_R$ scalar doublet χ_R to break $SU(2)_R \times U(1)_{B-L}$ to $U(1)_Y$ and a scalar bidoublet ϕ that breaks $SU(2)_L \times U(1)_Y$ down to $U(1)_{\text{em}}$, where the hypercharge Y is defined by $Y/2 = I_R^3 + (B-L)/2$, and I_R^3 is the third component of the right isospin. The detailed quantum numbers of the

fermions and Higgs bosons are presented in Table I. Also, in order to forbid a mixing mass term $M\bar{S}_1^c S_2$ that could

Fields	$Q_L = \begin{pmatrix} u_L \\ d_L \end{pmatrix}$	$Q_R = \begin{pmatrix} u_R \\ d_R \end{pmatrix}$	$L_L = \begin{pmatrix} \nu_L \\ e_L \end{pmatrix}$	$L_R = \begin{pmatrix} \nu_R \\ e_R \end{pmatrix}$	S_1	S_2	$\phi = \begin{pmatrix} \phi_1^0 & \phi_1^+ \\ \phi_2^- & \phi_2^0 \end{pmatrix}$	$\chi_R = \begin{pmatrix} \chi_R^+ \\ \chi_R^0 \end{pmatrix}$
\mathbb{G}_{LR}	$(\mathbf{3}, \mathbf{2}, \mathbf{1}, \frac{1}{3})$	$(\mathbf{3}, \mathbf{1}, \mathbf{2}, \frac{1}{3})$	$(\mathbf{1}, \mathbf{2}, \mathbf{1}, -1)$	$(\mathbf{1}, \mathbf{1}, \mathbf{2}, -1)$	$(\mathbf{1}, \mathbf{1}, \mathbf{1}, -2)$	$(\mathbf{1}, \mathbf{1}, \mathbf{1}, 2)$	$(\mathbf{1}, \mathbf{2}, \mathbf{2}, 0)$	$(\mathbf{1}, \mathbf{1}, \mathbf{2}, 1)$

TABLE I. The LRIS particle content and its representations and quantum numbers with respect to the LR gauge group $\mathbb{G}_{\text{LR}} = SU(3)_C \times SU(2)_L \times SU(2)_R \times U_{B-L}$.

spoil the IS mechanism, as discussed in [24], a Z_2 discrete symmetry is used, where all particles have even charges except S_1 , which has an odd charge. Based on the above particles and their charge assignments, the most general left-right symmetric Yukawa Lagrangian accounting for the scalar-fermion interactions and containing the IS neutrino mass terms is given by

$$\mathcal{L}_Y = \sum_{i,j=1}^3 y_{ij}^L \bar{L}_{Li} \phi L_{Rj} + \tilde{y}_{ij}^L \bar{L}_{Li} \tilde{\phi} L_{Rj} + y_{ij}^Q \bar{Q}_{Li} \phi Q_{Rj} + \tilde{y}_{ij}^Q \bar{Q}_{Li} \tilde{\phi} Q_{Rj} + y_{ij}^S \bar{L}_{Ri} \tilde{\chi}_R S_{2j}^c + H.c., \quad (1)$$

where $i, j = 1 \dots 3$ are family indices, $\tilde{\phi}$ is the dual bidoublet of the scalar bidoublet ϕ , defined as $\tilde{\phi} = \tau_2 \phi^* \tau_2$, and $\tilde{\chi}_R$ is the dual doublet of the scalar doublet χ_R , given by $\tilde{\chi}_R = i\tau_2 \chi_R^*$. A detailed discussion on the Higgs potential and the associated VEVs will be given in the next section. Here, we assume a nonvanishing VEV of χ_R , $\langle \chi_R \rangle = v_R / \sqrt{2}$ of an order TeV to break the right-handed electroweak sector together with $B-L$. In addition, the VEVs of ϕ , given by $\langle \phi \rangle = \text{diag}(k_1 / \sqrt{2}, k_2 / \sqrt{2})$, are of an order $\mathcal{O}(100)$ GeV to break the electroweak symmetry of the SM.

After $B-L$ symmetry breaking, a small mass term $\mu_s \bar{S}_2^c S_2$ (and plausibly $\mu'_s \bar{S}_1^c S_1$) is generated from a nonrenormalizable term (of dimension seven $\propto \chi_R^4 \bar{S}_2^c S_2 / M^3$), which implies that $\mu_s = \lambda_s v_R^4 / M^3 \lesssim \mathcal{O}(1)$ KeV [25], where λ_s is an interaction effective dimensionless coupling. For $v_R \sim \mathcal{O}(10^3)$ GeV, one finds that $\mu_s \sim \mathcal{O}(10^{-7})$ GeV if $\lambda_s / M^3 \sim \mathcal{O}(10^{-19})$ GeV. Thus, if $\lambda_s \sim \mathcal{O}(1)$, the nonrenormalizable scale M is an intermediate scale, namely $M \sim \mathcal{O}(10^3)$ TeV. While for $\lambda_s \sim \mathcal{O}(10^{-3})$, one finds $M \sim \mathcal{O}(10)$ TeV. As a result, the Lagrangian of neutrino masses is given by

$$\mathcal{L}_m^\nu = M_D \bar{\nu}_L \nu_R + M_R \bar{\nu}_R^c S_2 + \mu_s \bar{S}_2^c S_2 + H.c., \quad (2)$$

where the 3×3 matrix $M_D = v(y^L s_\beta + \tilde{y}^L c_\beta) / \sqrt{2}$ is the Dirac neutrino mass matrix and the 3×3 matrix $M_R = y^s v_R / \sqrt{2}$. This is the standard neutrino IS matrices [15–18]. Here, we have fixed the VEVs $k_{1,2}$ such that $v^2 = k_1^2 + k_2^2$ and $k_1 = v s_\beta$, $k_2 = v c_\beta$, where we define $s_x = \sin x$, $c_x = \cos x$, and $t_x = \tan x$, henceforth. In this regard, the following 9×9 neutrino mass matrix can be written as $\bar{\psi}^c \mathcal{M}_\nu \psi$ with the flavor basis $\psi = (\nu_L^c, \nu_R, S_2)$ and

$$\mathcal{M}_\nu = \begin{pmatrix} 0 & M_D & 0 \\ M_D^T & 0 & M_R \\ 0 & M_R^T & \mu_s \end{pmatrix}. \quad (3)$$

The diagonalization of this mass matrix leads to the physical light and heavy neutrino states ν_{ℓ_i}, ν_{h_j} , $i = 1 \dots 3$, $j = 1 \dots 6$, with the following mass eigenvalues:

$$m_{\nu_{\ell_i}} = M_D M_R^{-1} \mu_s (M_R^T)^{-1} M_D^T, \quad i = 1 \dots 3, \quad (4)$$

$$m_{\nu_{h_j}}^2 = M_R^2 + M_D^2, \quad j = 1 \dots 6. \quad (5)$$

On the other hand, after electroweak symmetry breaking, quarks and charged leptons acquire their masses via Higgs

mechanism, as follows:

$$M_u = \frac{v}{\sqrt{2}}(y^Q s_\beta + \tilde{y}^Q c_\beta), \quad (6)$$

$$M_d = \frac{v}{\sqrt{2}}(y^Q c_\beta + \tilde{y}^Q s_\beta), \quad (7)$$

$$M_\ell = \frac{v}{\sqrt{2}}(y^L c_\beta + \tilde{y}^L s_\beta). \quad (8)$$

In contrast to the SM, fermions acquire their masses from different VEVs sources as shown in Eqs. (6)-(8). This allows the existence of a tree-level FCNC induced by neutral Higgs bosons exchange between different fermion families, which is severely constrained by experiments [26]. The physical fermions' masses are given after diagonalization by

$$M_u^{\text{diag}} = V_L^{u\dagger} M'^u V_R^u, \quad M_d^{\text{diag}} = V_L^{d\dagger} M'^d V_R^d, \quad M_\ell^{\text{diag}} = V_L^{\ell\dagger} M'^\ell V_R^\ell. \quad (9)$$

In this case, the quark Yukawa couplings can be written as

$$y^Q = -\frac{\sqrt{2}}{vc_{2\beta}}(s_\beta V_L^u M^u V_R^{u\dagger} - c_\beta V_L^d M^d V_R^{d\dagger}), \quad (10)$$

$$\tilde{y}^Q = -\frac{\sqrt{2}}{vc_{2\beta}}(c_\beta V_L^u M^u V_R^{u\dagger} - s_\beta V_L^d M^d V_R^{d\dagger}). \quad (11)$$

These Yukawa couplings lead to the following interactions between quarks and neutral Higgs bosons

$$\begin{aligned} \mathcal{L}_{\text{int}} = & \frac{-\sqrt{2}}{vc_{2\beta}} \left[\bar{u}_L (M_u^{\text{diag}}(s_\beta \phi_1^0 - c_\beta \phi_2^{0*}) + V_{\text{CKM}}^L M_d^{\text{diag}} V_{\text{CKM}}^R (-c_\beta \phi_1^0 + s_\beta \phi_2^{0*})) u_R \right] \\ & - \frac{\sqrt{2}}{vc_{2\beta}} \left[\bar{d}_L (M_d^{\text{diag}}(s_\beta \phi_1^0 - c_\beta \phi_2^{0*}) + V_{\text{CKM}}^L M_u^{\text{diag}} V_{\text{CKM}}^R (-c_\beta \phi_1^0 + s_\beta \phi_2^{0*})) d_R \right], \end{aligned} \quad (12)$$

where $V_{\text{CKM}}^{L,R} = V_{L,R}^{u\dagger} V_{L,R}^d$ are the mixing matrices for left and right quarks, respectively. It is clearly that the second nondiagonal terms in the above equations are sources of FCNC, which could be quite dangerous if one considers V_{CKM}^R with large off diagonal entries. We assume that our LR model is derived from a GUT model, like $SO(10)$; therefore a universal gauge coupling is naturally adopted: $g_L = g_R$. Furthermore, we consider a truly minimal Higgs sector made up of one bidoublet ϕ and one RH doublet χ_R . As shown in [27, 28], in this class of models with $g_L = g_R$, the RH-mixing matrix V_{CKM}^R can be calculated in terms of the LH-mixing matrix V_{CKM}^L and $V_{\text{CKM}}^R \simeq V_{\text{CKM}}^L$, at the leading order. As a result, the flavor violation is under control and no longer dangerous, because it will be proportional to some power of the Wolfenstein parameter. $\lambda \sim 0.12$ [29, 30]. For example, the $b-s$ FCNC transition via a neutral Higgs boson H_i ($i = 1 \dots 3$) will be proportional to $(V_{\text{CKM}}^L)_{3i} (M_u^{\text{diag}})_{ii} (V_{\text{CKM}}^R)_{i2} = (V_{\text{CKM}}^L)_{3i} (M_u^{\text{diag}})_{ii} (V_{\text{CKM}}^L)_{i2}$. Thus, with the neutral Higgs mixing $Z_{ij}^H < 1$, one finds that $\frac{1}{vc_{2\beta}}(-c_\beta Z_{i1}^H + s_\beta Z_{i2}^H)(m_u \lambda^4 + m_c \lambda^2 + m_t \lambda^2) \ll \lambda^2$, which is small enough and does not generate any conflict with recent experimental observations [26, 31].

Now we turn to the gauge sector. The scalar bidoublet ϕ mixes the left and right gauge bosons. Thus, one can show that the symmetric mass matrix for neutral left, right and $B-L$ gauge bosons basis $(W_{R\mu}^3, V_\mu, W_{L\mu}^3)$, is given by

$$M_{ZZ'}^2 = \frac{1}{4} \begin{pmatrix} g_R^2(v_R^2 + v^2) & -g_{BL}g_R v_R^2 & -g_L g_R v^2 \\ \cdot & g_{BL}^2 v_R^2 & 0 \\ \cdot & \cdot & g_L^2 v^2 \end{pmatrix}. \quad (13)$$

Notice that we exploit the symmetry of the matrix to write dots for the lower off diagonal elements instead of repeating them through the text. After the first stage of left-right symmetry breaking down to the SM symmetry, both the right and $B-L$ gauge bosons $W_{R\mu}^3$ and V_μ mix with an angle φ whose $s_\varphi = g_{BL}/\sqrt{g_R^2 + g_{BL}^2}$ to give the massless hypercharge $U(1)_Y$ gauge boson B_μ , while the right neutral gauge boson $Z_{R\mu}$ becomes massive. Then, the SM gauge symmetry is broken and $W_{L\mu}^3$, and B_μ mix with the Weinberg angle $\sin \theta_w \equiv s_w = e/g_L$ and give the photon A_μ and

the left weak boson $Z_{L\mu}$. However, both $Z_{L\mu}$ and $Z_{R\mu}$ mix by the scalar bidoublet ϕ , as mentioned above, and give the physical states of Z_μ and Z'_μ bosons as follows

$$\begin{pmatrix} Z_{R\mu} \\ B_\mu \end{pmatrix} = \begin{pmatrix} c_\varphi & -s_\varphi \\ s_\varphi & c_\varphi \end{pmatrix} \begin{pmatrix} W_{R\mu}^3 \\ V_\mu \end{pmatrix}, \quad \begin{pmatrix} Z_{L\mu} \\ A_\mu \end{pmatrix} = \begin{pmatrix} c_w & -s_w \\ s_w & c_w \end{pmatrix} \begin{pmatrix} W_{L\mu}^3 \\ B_\mu \end{pmatrix}, \quad \begin{pmatrix} Z_\mu \\ Z'_\mu \end{pmatrix} = \begin{pmatrix} c_\vartheta & -s_\vartheta \\ s_\vartheta & c_\vartheta \end{pmatrix} \begin{pmatrix} Z_{L\mu} \\ Z_{R\mu} \end{pmatrix}. \quad (14)$$

This leads to the total mixing $(W_{R\mu}^3, V_\mu, W_{L\mu}^3)^T = Z^Z (Z'_\mu, Z_\mu, A_\mu)^T$, where $Z^{ZT} M_Z^2 Z^Z = \text{diag}(M_{Z'}^2, M_Z^2, 0)$ and the rotation matrix Z^Z is

$$Z^Z = \begin{pmatrix} c_\vartheta c_\varphi - s_\vartheta s_w s_\varphi & -s_\vartheta c_\varphi - c_\vartheta s_w s_\varphi & c_w s_\varphi \\ -c_\vartheta s_\varphi - s_\vartheta s_w c_\varphi & s_\vartheta s_\varphi - c_\vartheta s_w c_\varphi & c_w c_\varphi \\ s_\vartheta c_w & c_\vartheta c_w & s_w \end{pmatrix}, \quad (15)$$

where the $Z - Z'$ mixing angle ϑ is given by

$$\tan 2\vartheta = \frac{2M_{LR}}{M_{LL} - M_{RR}} = \frac{2g_2^3 \sqrt{g_2^2 + 2g_{BL}^2}}{(g_2^2 + g_{BL}^2)^2 (\frac{v_R}{v})^2 - 2g_2^2 g_{BL}^2}, \quad (16)$$

and the $(Z_{L\mu}, Z_{R\mu})$ symmetric mass matrix elements are

$$M_{LL} = \frac{g_2^2 v^2 (g_2^2 + 2g_{BL}^2)}{4(g_2^2 + g_{BL}^2)}, \quad (17)$$

$$M_{LR} = M_{RL} = \frac{-g_2^3 v^2 \sqrt{g_2^2 + 2g_{BL}^2}}{4(g_2^2 + g_{BL}^2)}, \quad (18)$$

$$M_{RR} = \frac{g_2^4 v^2 + (g_2^2 + g_{BL}^2)^2 v_R^2}{4(g_2^2 + g_{BL}^2)}. \quad (19)$$

The mass eigenvalues are given by

$$M_{Z,Z'}^2 = \frac{1}{2} (M_{LL} + M_{RR} \mp (M_{RR} - M_{LL}) \sqrt{1 + \tan^2 2\vartheta}). \quad (20)$$

The LHC search for the Z' gauge boson is rather model dependent; in our case, we found that the following limits are imposed on $M_{Z'}$: $0.8 \lesssim M_{Z'} \lesssim 4.5$ TeV [32, 33].

The charged gauge boson symmetric mass matrix in basis $(W_{L\mu}^\pm, W_{R\mu}^\pm)$ is given by

$$M_{WW'}^2 = \frac{1}{4} \begin{pmatrix} g_L^2 v^2 & -g_L g_R v^2 s_{2\beta} \\ . & g_R^2 (v^2 + v_R^2) \end{pmatrix}. \quad (21)$$

Thus, the $W - W'$ diagonalization mixing angle ξ is

$$\tan 2\xi = \frac{2g_L g_R s_{2\beta}}{g_R^2 (1 + (\frac{v_R}{v})^2) - g_L^2}, \quad (22)$$

and the physical gauge bosons masses $M_{W,W'}$ are approximately

$$M_{W,W'}^2 = \frac{1}{8} (g_L^2 v^2 + g_R^2 (v^2 + v_R^2) \mp (g_R^2 (v^2 + v_R^2) - g_L^2 v^2) \sqrt{1 + \tan^2 2\xi}). \quad (23)$$

or approximately with $g_L = g_R$,

$$M_W = \frac{g_2 v}{2}, \quad M_{W'} = \frac{g_2 \sqrt{v^2 + v_R^2}}{2}. \quad (24)$$

The LHC's direct searches for W' impose stringent constraints on $M_{W'}$. These constraints, however, are model dependent, as they are determined by the assumptions imposed on the gauge couplings and the dominated channels of W' decays. In the LR model, the decay channel of W' to ν_R may be dominant, suppressing other decay channels to SM leptons or quarks. As a result, the bounds on $M_{W'}$ are relaxed, as highlighted in Ref. [34]. In this case, a conservative bound on the mass of the gauge boson W' is of order 2 TeV.

III. HIGGS SECTOR IN THE LRIS

As mentioned in the previous section, the Higgs sector of the LRIS consists of a bidoublet ϕ and a right doublet χ_R as in Table I, and the gauge symmetries $SU(2)_R \times U(1)_{B-L}$ are spontaneously broken to $U(1)_Y$ through the VEV of χ_R , then the $SU(2)_L \times U(1)_Y$ symmetries are broken by VEVs of ϕ . The most general Higgs potential that is invariant under the above mentioned symmetries (gauge and discrete) is given by [12]

$$\begin{aligned} V(\phi, \chi_R) = & \mu_1 \text{Tr}(\phi^\dagger \phi) + \mu_2 [\text{Tr}(\tilde{\phi} \phi^\dagger) + \text{Tr}(\tilde{\phi}^\dagger \phi)] + \lambda_1 (\text{Tr}(\phi^\dagger \phi))^2 + \lambda_2 [(\text{Tr}(\tilde{\phi} \phi^\dagger))^2 + (\text{Tr}(\tilde{\phi}^\dagger \phi))^2] \\ & + \lambda_3 \text{Tr}(\tilde{\phi} \phi^\dagger) \text{Tr}(\tilde{\phi}^\dagger \phi) + \lambda_4 \text{Tr}(\phi \phi^\dagger) (\text{Tr}(\tilde{\phi} \phi^\dagger) + \text{Tr}(\tilde{\phi}^\dagger \phi)) + \mu_3 (\chi_R^\dagger \chi_R) + \rho_1 (\chi_R^\dagger \chi_R)^2 \\ & + \alpha_1 \text{Tr}(\phi^\dagger \phi) (\chi_R^\dagger \chi_R) + \alpha_2 (\chi_R^\dagger \phi^\dagger \phi \chi_R) + \alpha_3 (\chi_R^\dagger \tilde{\phi}^\dagger \tilde{\phi} \chi_R) + \alpha_4 (\chi_R^\dagger \phi^\dagger \tilde{\phi} \chi_R + H.c.). \end{aligned} \quad (25)$$

It is worth mentioning here that the potential parameters in (25) are constrained by the spectrum and minimization and boundedness from below conditions of the potential provided in Appendixes VIA and VIB.

A. Higgs masses and mixing

It is worth noting that before symmetry breaking there were 12 scalar degrees of freedom: 8 of ϕ and 4 of χ_R . After symmetry breaking, two neutral components and four charged components of these degrees of freedom are eaten by the neutral gauge bosons: Z_μ and Z'_μ and the charged gauge bosons: W_μ^\pm and $W'_\mu{}^\pm$ to acquire their masses, respectively. Therefore in this class of models, six scalars remain as physical Higgs bosons; as we show, two of them are charged Higgs bosons, one is a pseudoscalar Higgs boson, and the remaining three give CP -even neutral Higgs bosons.

1. Charged Higgs bosons

It can be easily seen that the symmetric mass matrix of the charged Higgs bosons in the basis $(\phi_1^\pm, \phi_2^\pm, \chi_R^\pm)$ is given by

$$M_{H^\pm}^2 = \frac{\alpha_{32}}{2} \begin{pmatrix} \frac{v_R^2 s_\beta^2}{c_{2\beta}} & \frac{v_R^2 s_{2\beta}}{2c_{2\beta}} & -vv_R s_\beta \\ \cdot & \frac{v_R^2 c_\beta^2}{c_{2\beta}} & -vv_R c_\beta \\ \cdot & \cdot & v^2 c_{2\beta} \end{pmatrix}. \quad (26)$$

Notice that since $s_\beta \ll 1$, the entries of the above matrix are of following orders: $(M_{H^\pm}^2)_{11} \ll v_R^2$, $(M_{H^\pm}^2)_{22} \approx v_R^2$ and $(M_{H^\pm}^2)_{33} \approx v^2$, while the off diagonal elements are given by $(M_{H^\pm}^2)_{12} \ll v_R^2$, $(M_{H^\pm}^2)_{13} \lesssim vv_R$ and $(M_{H^\pm}^2)_{23} \approx vv_R$. The matrix $M_{H^\pm}^2$ can be diagonalized by a unitary matrix,

$$Z^{H^\pm} = \begin{pmatrix} \frac{vc_{2\beta}}{\sqrt{v^2 c_{2\beta}^2 + v_R^2 s_\beta^2}} & 0 & \frac{v_R s_\beta}{\sqrt{v^2 c_{2\beta}^2 + v_R^2 s_\beta^2}} \\ -\frac{\frac{1}{2}v_R^2 s_{2\beta}}{\sqrt{(v^2 c_{2\beta}^2 + v_R^2 s_\beta^2)(v^2 c_{2\beta}^2 + v_R^2)}} & \sqrt{\frac{v^2 c_{2\beta}^2 + v_R^2 s_\beta^2}{v^2 c_{2\beta}^2 + v_R^2}} & \frac{vv_R c_\beta c_{2\beta}}{\sqrt{(v^2 c_{2\beta}^2 + v_R^2 s_\beta^2)(v^2 c_{2\beta}^2 + v_R^2)}} \\ -\frac{v_R s_\beta}{\sqrt{v^2 c_{2\beta}^2 + v_R^2}} & -\frac{v_R c_\beta}{\sqrt{v^2 c_{2\beta}^2 + v_R^2}} & \frac{vc_{2\beta}}{\sqrt{v^2 c_{2\beta}^2 + v_R^2}} \end{pmatrix}, \quad (27)$$

such that $Z^{H^\pm} M_{H^\pm}^2 Z^{H^\pm T} = \text{diag}(0, 0, m_{H^\pm}^2)$ and $(\phi_1^\pm, \phi_2^\pm, \chi_R^\pm)^T = Z^{H^\pm T} (G_1^\pm, G_2^\pm, H^\pm)^T$, where G_1^\pm and G_2^\pm are the charged Goldstone bosons eaten by the charged gauge bosons W_μ and W'_μ to acquire their masses via the Higgs mechanism. In addition, it remains one massive eigenstate of a physical charged Higgs boson H^\pm , with the following mass:

$$m_{H^\pm}^2 = \frac{\alpha_{32}}{2} \left(\frac{v_R^2}{c_{2\beta}} + v^2 c_{2\beta} \right), \quad (28)$$

where $\alpha_{32} = \alpha_3 - \alpha_2$. Thus, if $v_R \sim \mathcal{O}(\text{TeV})$ and $\alpha_{32} \sim \mathcal{O}(10^{-2})$, then the charged Higgs boson mass is on the order of hundreds GeV as in Table II. The physical charged Higgs boson is given through the rotation matrix Z^{H^\pm} by

$$H^\pm = Z_{13}^{H^\pm} \phi_1^\pm + Z_{23}^{H^\pm} \phi_2^\pm + Z_{33}^{H^\pm} \chi_R^\pm, \quad (29)$$

where $Z_{13}^{H^\pm} \approx 1$, while $Z_{23}^{H^\pm} \approx v/(v_R t_\beta) < 1$ and $Z_{33}^{H^\pm} \approx v/v_R \ll 1$. Therefore, the charged Higgs boson is mainly made of ϕ_1^\pm .

2. CP -odd Higgs bosons

Now, we consider the neutral scalar fields and their masses. This can be obtained if one fluctuates the neutral components of the bidoublet ϕ and the doublet χ_R around their vacua as follows:

$$\phi_i^0 = \frac{1}{\sqrt{2}}(v_i + \phi_i^{0R} + i\phi_i^{0I}), \quad (30)$$

where $\phi_i = \phi_{1,2}, \chi_R$ and $v_i = k_{1,2}, v_R$. In this case, the symmetric mass matrix of the CP -odd Higgs bosons is given by

$$(M_A^2)_{ij} = \left. \frac{\partial^2 V(\phi, \chi_{L,R})}{\partial \phi_i^{0I} \partial \phi_j^{0I}} \right|_{\langle \phi_{i,j}^{0R} \rangle = \langle \phi_{i,j}^{0I} \rangle = 0}. \quad (31)$$

Therefore, in the basis $(\phi_1^{0I}, \phi_2^{0I}, \chi_R^{0I})$, the pseudoscalar Higgs bosons mass matrix is given by

$$M_A^2 = \frac{1}{2} \left(\frac{v_R^2 \alpha_{32}}{c_{2\beta}} - 4v^2(2\lambda_2 - \lambda_3) \right) \begin{pmatrix} c_\beta^2 & s_\beta c_\beta & 0 \\ \cdot & s_\beta^2 & 0 \\ \cdot & \cdot & 0 \end{pmatrix}, \quad (32)$$

which can be diagonalized by a unitary matrix,

$$Z^A = \begin{pmatrix} 0 & 0 & 1 \\ -s_\beta & c_\beta & 0 \\ c_\beta & s_\beta & 0 \end{pmatrix}, \quad (33)$$

such that $Z^A M_A^2 Z^{AT} = \text{diag}(0, 0, m_A^2)$ and $(\phi_1^{0I}, \phi_2^{0I}, \chi_R^{0I})^T = Z^{AT}(G_1^0, G_2^0, A)^T$, where G_1^0 and G_2^0 are the neutral Goldstone bosons eaten by the two neutral gauge bosons Z_μ and Z'_μ to acquire their masses, and the following nonzero eigenvalue is the physical mass of the pseudoscalar boson A ,

$$m_A^2 = \frac{1}{2} \left(\frac{v_R^2}{c_{2\beta}} \alpha_{32} - 4v^2(2\lambda_2 - \lambda_3) \right). \quad (34)$$

Thus, for $v_R \sim \mathcal{O}(\text{TeV})$ and $\alpha_{32} \sim \mathcal{O}(10^{-2})$, the pseudoscalar Higgs boson mass is on the order of a few hundred GeVs, as well as in Table II. The physical pseudoscalar Higgs boson is given through the rotation matrix Z^A by

$$A = c_\beta \phi_1^{0I} + s_\beta \phi_2^{0I}. \quad (35)$$

According to our choice $s_\beta \ll 1$ and $A \approx \phi_1^{0I}$.

3. CP -even Higgs bosons

Finally, we consider the CP -even Higgs bosons. Similar to the CP -odd Higgs bosons, the (3×3) symmetric mass matrix of CP -even Higgs bosons is given by

$$(M_H^2)_{ij} = \left. \frac{\partial^2 V(\phi, \chi_{L,R})}{\partial \phi_i^{0R} \partial \phi_j^{0R}} \right|_{\langle \phi_{i,j}^{0R} \rangle = \langle \phi_{i,j}^{0I} \rangle = 0}, \quad (36)$$

with the elements

$$m_{11} = 2v^2(\lambda_1 s_\beta^2 + \lambda_{23} c_\beta^2 + \lambda_4 s_{2\beta}) + \frac{1}{4}(\frac{1}{c_{2\beta}} + 1)\alpha_{32}v_R^2, \quad (37)$$

$$m_{12} = m_{21} = v^2((\lambda_1 + \lambda_{23})s_{2\beta} + 2\lambda_4) - \frac{1}{4}\alpha_{32}v_R^2 t_{2\beta}, \quad (38)$$

$$m_{13} = m_{31} = vv_R(\alpha_{13}s_\beta + \alpha_4 c_\beta), \quad (39)$$

$$m_{22} = 2v^2(\lambda_1 c_\beta^2 + \lambda_{23} s_\beta^2 + \lambda_4 s_{2\beta}) + \frac{1}{4}(\frac{1}{c_{2\beta}} - 1)\alpha_{32}v_R^2, \quad (40)$$

$$m_{23} = m_{32} = vv_R(\alpha_{12}c_\beta + \alpha_4 s_\beta), \quad (41)$$

$$m_{33} = 2\rho_1 v_R^2, \quad (42)$$

where $\alpha_{1i} = \alpha_1 + \alpha_i$, $i = 2, 3$ and $\lambda_{23} = 2\lambda_2 + \lambda_3$. This matrix can be diagonalized by a unitary transformation matrix Z^H such that $Z^H M_H^2 Z^{HT} = \text{diag}(m_{H_1}^2, m_{H_2}^2, m_{H_3}^2)$ and $(\phi_1^{0R}, \phi_2^{0R}, \chi_R^{0R})^T = Z^{HT}(H_1, H_2, H_3)^T$. The coefficients of the rotation matrix Z^H are given explicitly in Appendix VIC. After rotation, we obtain three massive neutral Higgs bosons

$$H_i = Z_{ij}^H \phi_j^{0R}. \quad (43)$$

Here, a few remarks are in order (for $t_\beta \ll 1$): (i) To obtain the SM-like Higgs boson h and another Higgs boson h' of order of a few GeVs we take $\lambda_1 \sim \mathcal{O}(10^{-1})$ and $\alpha_{32} \sim \mathcal{O}(10^{-2})$ so that $m_{11}, m_{22} \sim \mathcal{O}(\text{GeV}^2)$. (ii) Taking $\rho_1 \sim \mathcal{O}(10^{-1})$ alongside $\alpha_{32} \sim \mathcal{O}(10^{-2})$ leads to small mixing between χ_R^{0R} and the bidoublet components $\phi_{1,2}^{0R}$ such that $m_{13}^2/(m_{11}m_{33}) \ll 1$ and $m_{23}^2/(m_{22}m_{33}) \ll 1$. This leads to the small mixing of χ_R^{0R} and the light states h, h' and small mixing between the heaviest state H_3 and the bidoublet components $\phi_{1,2}^{0R}$, i.e., $Z_{13}^H, Z_{23}^H, Z_{31}^H, Z_{32}^H \sim \mathcal{O}(10^{-2} - 10^{-1}) \ll 1$, as in Table III. Thus, the heaviest Higgs boson $H_3 \sim \chi_R^{0R}$ with a mass $m_{H_3}^2 \approx m_{33}$. (iii) Moreover, if we assume that $\lambda_{23} \geq \lambda_1$, one finds that $m_{11} > m_{22}$ and $m_{12}^2/(m_{11}m_{22}) \ll 1$, which implies that the mixing $Z_{11}^H, Z_{22}^H \sim \mathcal{O}(10^{-2} - 10^{-1}) < 1$ as in Table III. Accordingly, the SM-like Higgs boson can be defined as $H_1 \sim \phi_2^{0R}$ and the next lightest Higgs boson is given by $H_2 \sim \phi_1^{0R}$, with masses $m_{H_1}^2 \approx m_{22} - m_{12}^2/(m_{11} - m_{22}) < m_{H_2}^2 \approx m_{11} + m_{12}^2/(m_{11} - m_{22})$. In addition, this keeps the SM-like Higgs couplings with the SM fermions and gauge bosons intact. (iv) For small values of λ_4 , one finds that H_1 could be the lightest while H_2 may represent the SM-like Higgs boson. However, for most of the parameter space ($\lambda_4, \alpha_{32}, t_\beta$) we have H_1 as the SM-like Higgs boson, and this is what we adopted here as in Eq. (46) below. (v) Due to the mass hierarchy considered here, values of $\alpha_{12,13}$ and α_4 are not constrained for the mass spectrum. But in our LHC analysis below, we see that large values of α_4 and λ_4 , as in Eq. (46) and Table II, are preferable for large coupling $g_{h'h h}$ in Eq. (48), and hence for large $\sigma(h' \rightarrow hh)$. Lastly, we should mention here that all parameters are constrained by the copositivity conditions of Appendix VIB.

As emphasized, the lightest eigenstate $H_1 \equiv h$ will be the SM-like Higgs boson that we fix its mass with $m_h = 125$ GeV [35, 36]. This condition can be used to fix the value of one of the involved parameters, λ_1 . The other two eigenvalues are given by

$$m_{H_{2,3}}^2 = \frac{1}{2} \left(T^h - m_h^2 \mp \sqrt{(T^h - m_h^2)^2 - \frac{4D^h}{m_h^2}} \right), \quad (44)$$

where the trace T^h of the Higgs matrix M_H^2 is

$$T^h = \text{Tr}(M_H^2) = 2v^2(\lambda_1 + \lambda_{23} + 2\lambda_4 s_{2\beta}) + (\frac{\alpha_{32}}{2c_{2\beta}} + 2\rho_1)v_R^2, \quad (45)$$

and D^h is the determinant of M_H^2 , which is explicitly given in Appendix VIC. From Eq. (44), one can show that the next lightest CP -even neutral Higgs boson, $H_2 \equiv h'$, could have a mass of order a few hundred GeVs, as shown in Fig. 1 (left). In this figure, $m_{h'}$ is given as function of α_{32} , which is one of the relevant parameters

in the scalar potential, with choosing $\lambda_{23} \in [-0.1, 3]$ and varying other parameters in the following ranges upon our discussion above:

$$\lambda_1 \in [0.18, 0.30], \quad \lambda_4 \in [0.70, 0.99], \quad \alpha_1 \in [0.06, 0.16], \quad \alpha_4 \in [0.60, 0.99], \quad \rho_1 \in [0.08, 0.14]. \quad (46)$$

Moreover, a huge scan over the parameter space of the LRIS was conducted taking into account the recent LHC constraints using integratively HIGGSBOUNDS and HIGGSIGNALS programs as explained below [37, 38]. The scan confirmed our previous discussions and ranges considered. We chose the three benchmark points in Table II with optimized cross sections in both signals of interest in our analysis below. We also considered our h' in the three mass ranges $m_{h'} = 250, 400$ GeV and 600 GeV. In Fig. 1 (left), we circled the three benchmark points of Table II.

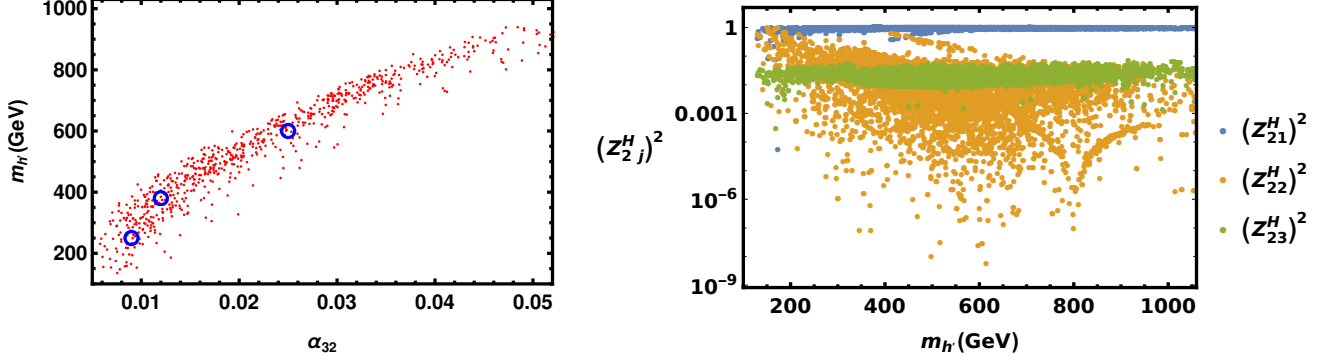


FIG. 1. Left: The next lightest Higgs boson mass $m_{h'}$ as a function of the most relevant parameter α_{32} . The three benchmark points under consideration of Table II are surrounded by blue circles. Right: h' mixing versus its mass $m_{h'}$. The other involved parameters are varied as in Eq. (46).

The interactions of h' with the SM fermions and gauge bosons, which are quite relevant for its search at the LHC, are given in terms of the mixing coupling Z_{2i}^H . As explained above, the physical eigenstate h' is given by the superposition of real parts of neutral components of scalar doublets as follows:

$$h' = Z_{21}^H \phi_1^{0R} + Z_{22}^H \phi_2^{0R} + Z_{23}^H \chi_R^{0R}. \quad (47)$$

In Fig. 1 (right), we display the mixing Z_{2i}^H versus $m_{h'}$ for the same set of parameters considered in Fig. 1 (left). As can be seen from this plot, h' is essentially generated from ϕ_1 with smaller contributions from the real components of ϕ_2 and χ_R .

Before closing this section, we highlight the relevant interaction couplings of h' with Z_μ gauge boson, $g_{h'ZZ}$, and with the SM-like Higgs boson, $g_{h'hh}$. These interactions are generated from kinetic terms and the scalar potential terms, respectively, and they are dominantly given by

$$g_{h'hh} \approx -2iZ_{21}^H Z_{12}^H \{v((\lambda_1 - \lambda_{23})c_\beta + 3\lambda_4 s_\beta)Z_{12}^H + \alpha_4 v_R Z_{13}^H\}, \quad (48)$$

$$g_{h'ZZ} \approx \frac{i}{2} g_2^2 v (c_\beta Z_{21}^H + s_\beta Z_{22}^H) (Z_{32}^Z - Z_{12}^Z)^2, \quad (49)$$

where Z^Z is the neutral gauge bosons mixing matrix, given in Eq. (15). We fix the gauge couplings as follows: $g_L = g_R = g_2 = 0.663$, $g_{BL} = 0.422$, the electroweak VEV as $v = 246$ GeV, and the Weinberg angle as $s_w^2 = 0.230$ [30]. In addition, the scale of LR symmetry breaking is fixed by $v_R = 6400$ GeV as given in Table II. Finally, the scalar potential parameters α_i , λ_i and ρ_1 are varied within the above mentioned ranges in Eq. (46). Also, one can show that the coupling $g_{h'ZZ}$ is typically smaller than the coupling $g_{h'hh}$. Therefore, probing h' through its ZZ -decay channel may not be promising, as it will be illustrated in the next section. In Table II, we fix the three benchmark points

Parameter	α_1	α_2	α_3	α_4	λ_1	λ_2	λ_3	λ_4	ρ_1	t_β	v_R (GeV)	m_{H^\pm} (GeV)	m_A (GeV)	$m_{h'}$ (GeV)	m_{H_3} (GeV)
BP1	0.133	0.155	0.164	0.833	0.215	0.316	-0.155	0.997	0.104	0.134	6400	440	315	250	3000
BP2	0.229	0.090	0.102	0.620	0.198	0.230	-0.104	0.917	0.117	0.159	6400	430	350	400	3100
BP3	0.118	0.168	0.193	0.957	0.228	0.309	-0.116	0.985	0.138	0.055	6400	700	650	600	3400

TABLE II. Benchmark points (BP) and corresponding Higgs spectrum used in figures and analysis of Sec. IV.

Mixing	Z_{11}^H	Z_{12}^H	Z_{13}^H	Z_{21}^H	Z_{22}^H	Z_{23}^H	Z_{31}^H	Z_{32}^H	Z_{33}^H
BP1	-0.135	0.989	-0.051	0.978	0.125	-0.166	0.158	0.072	0.985
BP2	-0.155	0.987	-0.051	0.982	0.148	-0.119	0.110	0.068	0.992
BP3	-0.065	0.997	-0.038	0.988	0.059	-0.141	0.138	0.047	0.989

TABLE III. Neutral Higgs mixing corresponding to the three BPs in Table II.

and their corresponding Higgs spectrum which are used in the LHC simulation analysis in Sec. IV, while Table III exhibits their corresponding neutral CP -even Higgs mixing.

It is noticeable that there are three effective parameters: α_{12} , α_{13} , and α_{23} involved in the above expressions. They are given in terms of the three parameters: α_1 , α_2 , and α_3 , so there is not any redundancy. Also, the effective parameter $\lambda_{23} = 2\lambda_2 + \lambda_3$ and $2\lambda_2 - \lambda_3$ (in the pseudoscalar mass) in terms of the two parameters λ_2 and λ_3 , and hence we have two independent parameters and there is no redundancy again. Finally, to satisfy the W' and Z' mass constraints, we should take $v_R \sim \text{TeV}$.

IV. SEARCH FOR HEAVY HIGGS BOSONS AT THE LHC

The heavy Higgs boson, h' , is mainly produced at the LHC from the gluon-gluon fusion (ggF) process, which induces about 90% of its total production cross section at the LHC. Other production mechanisms, like vector boson fusion (VBF), Higgs strahlung and Higgs production from top fusion associated with top quark, represent the remaining ratio of the h' production. In Fig. 2 (left), we show the h' ggF-production cross section versus $m_{h'}$ for the scanned values of parameters as in Eq. (46) and its preceding paragraph. It is noticeable from Fig. 2 (left) that the h' ggF production cross section $\sigma(pp \rightarrow h')$ can be of an order $\gtrsim 2$ pb for $m_{h'} \lesssim 400$ GeV. In this regard, we consider $L_{\text{int}} = 300 \text{ fb}^{-1}$ for relatively light h' and $L_{\text{int}} = 3000 \text{ fb}^{-1}$ for heavy h' and in different decay channels, at $\sqrt{s} = 14 \text{ TeV}$.

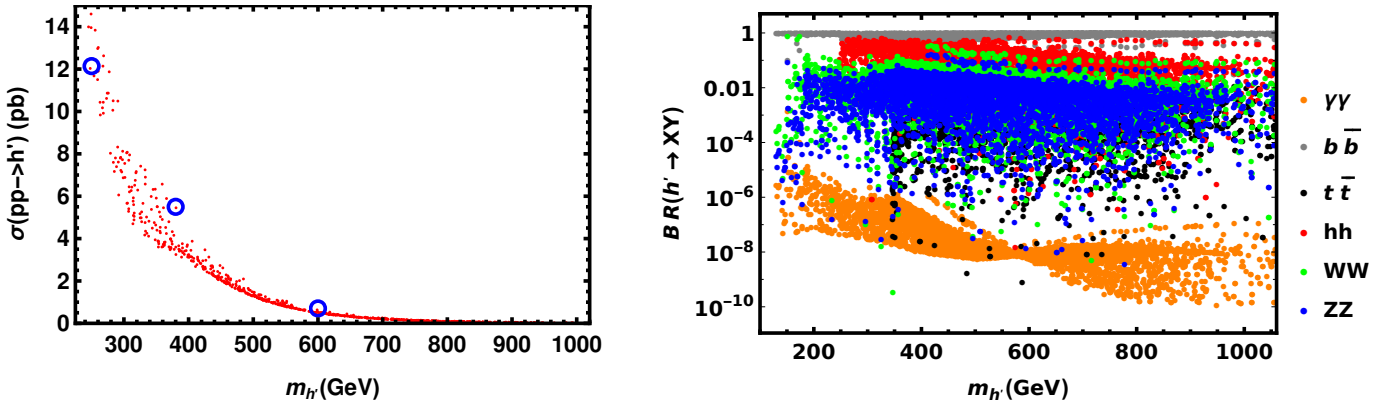


FIG. 2. Left: The h' production cross section from ggF as a function of its mass $m_{h'}$. The three benchmark points under consideration of Table II are surrounded by blue circles. Right: Branching ratios (BR) of h' decays versus its mass $m_{h'}$. The relevant parameters values are used as in Fig. 1.

We checked that all our benchmark points, given in Table II, are validated to satisfy the usual HIGGSBOUNDS and HIGGSSIGNALS limits confronted with the latest LHC data [37, 38]. Recall that HIGGSBOUNDS and HIGGSSIGNALS are testing Higgs sector both neutral and charged Higgs bosons of the model against the published exclusion bounds from Higgs searches at the LEP, Tevatron and LHC experiments. They are providing important tests for compatibility of any model beyond the SM.

Indeed, many HEP computational tools are used through this work from building the model analytically the way to the numerical manipulation. The LRIS model was first implemented into the SARAH package for building it, and it was then passed to SPHENO [39, 40] for numerical spectrum calculations. After that, the UFO model was used in MADGRAPH [41] for MONTECARLO events generation and matrix-element calculation. After that, PYTHIA was also used to simulate the initial and final state radiation, fragmentation, and hadronisation effects [42]. For detector simulation, the PYTHIA output was passed to DELPHES [43]. Finally, for data analysis, we used MADANALYSIS [44]. In Fig. 2 (right), we show the relevant h' decay branching ratios as functions of $m_{h'}$. It is remarkable to notice that for $m_{h'} \leq 600$ GeV, the h' decay branching ratio to two SM Higgs boson is not small, mainly $\text{BR}(h' \rightarrow hh) \geq 10\%$, which gives a hope for probing this heavy Higgs boson through this channel.

A. Search for h' Higgs boson in $h' \rightarrow hh \rightarrow b\bar{b}\gamma\gamma$

We began with the decay $h' \rightarrow hh \rightarrow b\bar{b}b\bar{b}$ for probing h' at the LHC, as the branching ratio $\text{BR}(h \rightarrow b\bar{b})$ is the largest of h decays. However, this process has a huge background and the signal is much lower than the relevant background, even for a quite heavy Higgs boson: $m_{h'} > 600$ GeV [45, 46] as in Fig. 3. We found that no set of cuts can be used to increase the statistical significance of the signal enough to overcome the corresponding background, as in Fig. 3. Specifically, we looked at the selection cuts for the following events on the pseudorapidity, the transverse momentum and the invariant mass of any combination of the four final states' b jets, respectively: $|\eta_{bb}| < 2.4$, $(P_T)_{bb} > 30.0$ GeV and $100.0 \text{ GeV} < M_{bb} < 150.0 \text{ GeV}$. Because our signal contains four final states b jets from a pair of on shell SM Higgs bosons, it is expected that the majority of the signal events occur within a window centred on the SM Higgs mass $100.0 \text{ GeV} < M_{bb} < 150.0 \text{ GeV}$. The corresponding relevant background events b -jets final states, on the other hand, are produced from a variety of other sources, the vast majority of which fall outside the above window. As a result, selecting events in this window is more likely to exclude events from the background than it is to exclude events from the signal. We examined all relevant signal and background kinematics and noticed that the used kinematics of η_{bb} , $(P_T)_{bb}$, M_{bb} are the only discriminators that can be used to overweight signal over background and that our choices optimized their usage based on cut efficiencies and the relative signal-to-background significance S/\sqrt{B} . Also, we applied the cuts used in the experimental references [45, 46] on $|\eta_b| < 2.5$ (2.4) and $(P_T)_b > 40$ (30) GeV of each single b jet of the final states but we found no hope to enhance the significance and it gave results much less than we obtained by the cuts we used above. We also looked at the decay process $h' \rightarrow hh \rightarrow 2b + 2W \rightarrow bbl\nu\ell\nu$, and we found that $\sigma(pp \rightarrow h' \rightarrow hh \rightarrow 2b + 2W \rightarrow bbl\nu\ell\nu) \sim \mathcal{O}(10^{-15})$ pb. This unusually small cross section is caused by various types of suppression for the corresponding amplitude. As a result, h' can not be probed through this channel even at high luminosity $L_{\text{int}} = 300, 3000 \text{ fb}^{-1}$ and small $m_{h'}$ [47, 48]. Therefore, in our analysis we are going to focus on the process $h' \rightarrow hh \rightarrow b\bar{b}\gamma\gamma$.

The on shell SM Higgs pair production from h' , followed by their decays $h' \rightarrow hh \rightarrow b\bar{b}\gamma\gamma$ is given by the Feynman diagram in Fig. 4. As mentioned, here we adapt the following different values of h' -mass: $m_{h'} = 250$ GeV, 400 GeV, and 600 GeV.

As the h' decay width $\Gamma_{h'}$ is much smaller than its mass, $\Gamma_{h'}/m_{h'} \ll 1$, the narrow width approximation can be used and the total cross section $\sigma(pp \rightarrow h' \rightarrow hh \rightarrow b\bar{b}\gamma\gamma)$ can be approximated as

$$\sigma(pp \rightarrow h' \rightarrow hh \rightarrow b\bar{b}\gamma\gamma) \approx \sigma(pp \rightarrow h') \times \text{BR}(h' \rightarrow hh) \times \text{BR}(h \rightarrow b\bar{b}) \times \text{BR}(h \rightarrow \gamma\gamma), \quad (50)$$

where the $h' \rightarrow hh$ decay branching ratio $\text{BR}(h' \rightarrow hh)$ is given in terms of the coupling $g_{h'hh}$ of Eq. (48). In Table IV the explicit values of the cross section and decay ratio of h' are presented for the three values of $m_{h'}$, under

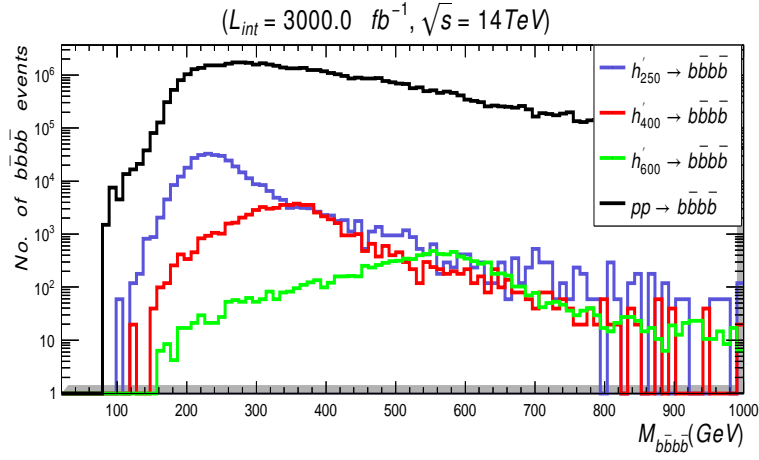


FIG. 3. Number of signals events for $h' \rightarrow b\bar{b}b\bar{b}$ decays at mass $m_{h'} = 250$ GeV (blue), 400 GeV (red), and 600 GeV (green) induced by the ggF versus the invariant mass of the final states $b\bar{b}b\bar{b}$, at $\sqrt{s} = 14$ TeV and $L_{\text{int}} = 3000 \text{ fb}^{-1}$ alongside the relevant background events (black) after applying the cut flow $|\eta| < 2.4$, $(P_T)_{bb} > 30.0$ and $100.0 < M_{bb} < 150.0$.

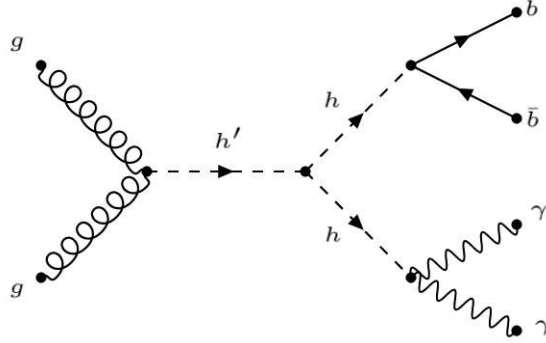


FIG. 4. Feynman diagram for the h' ggF production and decay process $gg \rightarrow h' \rightarrow hh \rightarrow b\bar{b}\gamma\gamma$.

consideration.

$m_{h'}$ (GeV)	$\sigma(pp \rightarrow h')$ (pb)	$\text{BR}(h' \rightarrow hh)$	$\sigma(pp \rightarrow h' \rightarrow hh \rightarrow b\bar{b}\gamma\gamma)$ (fb)
250	12.140	0.30	6.30
400	5.050	0.20	1.01
600	0.504	0.18	0.05

TABLE IV. $pp \rightarrow h'$ production cross section and its $h' \rightarrow hh$ decay branching ratio and the total cross section for its production and decay process $pp \rightarrow h' \rightarrow hh \rightarrow b\bar{b}\gamma\gamma$ for three different values of $m_{h'} = 250$ GeV, 400 GeV, and 600 GeV.

For potential discovery of h' at the LHC, we analyze both its signal and the corresponding relevant background from the SM processes. There are many reducible background processes [49]

$$pp \rightarrow b\bar{b}h\gamma\gamma/b\bar{b}j\gamma/b\bar{b}jj/cc\gamma\gamma/ccj\gamma/jj\gamma\gamma/ggh\gamma\gamma/tt/tt\gamma/tth\gamma\gamma/b\bar{b}z\gamma\gamma/zh\gamma\gamma. \quad (51)$$

The following preselection cuts at parton level are imposed in order to avoid any divergence in the parton-level calculations [49, 50]:

1. The pseudorapidity η of the two photons must be in acceptance of the detector so $|\eta_{\gamma\gamma}| \leq 2.4$.

2. The pseudorapidity η of the two jets must be in acceptance of the detector so $|\eta_{jj}| \leq 2.4$.
3. The transverse momentum P_T of the two jets satisfies $(P_T)_{jj} \geq 20$ GeV.
4. The transverse momentum P_T of the two photon satisfies $(P_T)_{\gamma\gamma} \geq 25$ GeV.

All these backgrounds can be reduced by appropriate kinematical cuts on pseudorapidity η_{ab} , transverse momentum $(P_T)_{ab}$, invariant mass M_{ab} of two final states objects a, b , and the angular distance $(\Delta R)_{ab}$ between a, b in the transverse plane, as specified in the cut flow tables below. The most relevant background processes which compete with our signal are the irreducible ones, $pp \rightarrow b\bar{b}\gamma\gamma$ and $pp \rightarrow zh \rightarrow b\bar{b}\gamma\gamma$. The later one can be also reduced down by the same set of cuts which are used in Table V. In Fig. 5, we show the number of signal events distributions for

Cuts (select)	Signal (S): $m_{h'} = 250$ GeV (400 GeV)	Background (B)	S/\sqrt{B}
Initial (no cut)	1904.00 (308.00)	25058.00	12.000 (1.950)
$M_{\gamma\gamma} > 119.5$ GeV	846.70 ± 21.70 (177.95 ± 8.82)	3015.10 ± 51.50	15.419 ± 0.00527 (3.241 ± 0.00272)
$M_{\gamma\gamma} < 130.5$ GeV	843.90 ± 19.30 (175.80 ± 8.36)	766.40 ± 19.20	30.430 ± 0.01500 (6.319 ± 0.01540)

TABLE V. Cut flow charts for the $h' \rightarrow hh \rightarrow b\bar{b}\gamma\gamma$ signal versus its relevant background and the corresponding number of events and significance at 300 fb^{-1} and $\sqrt{s} = 14$ TeV for $m_{h'} = 250$ GeV (400 GeV).

$m_{h'} = 250$ GeV and 400 GeV with the relevant irreducible background before (left) and after (right) applying cuts in Table V, respectively. In our signal, the final states kinematics are all boosted by the two on shell SM-like Higgs bosons and their distributions are narrowed and peaked around our h' windows. This behavior of signal events is unlike that of the background events where final states have many sources and their kinematics' distributions are usually broadened throughout the whole range of analysis. For this, we notice the high relative reduction of the background to our signal when we restrict our analysis on events of kinematics which are expected to be distributed about our h' as mentioned. We demand final state photons pairs of invariant masses as in Table V and this increases our signal significance in both cases of $m_{h'} = 250$ GeV, 400 GeV. This situation is shown in Fig. 5, where the signals are first much less than the relevant background (left) and choosing the certain cuts of Table V diminishes the background and makes the signals events finally dominate the background. The benchmark point with $m_{h'} = 600$ GeV is not included here as its cross section is quite tiny with the considered ($L_{\text{int}} = 300 \text{ fb}^{-1}$).

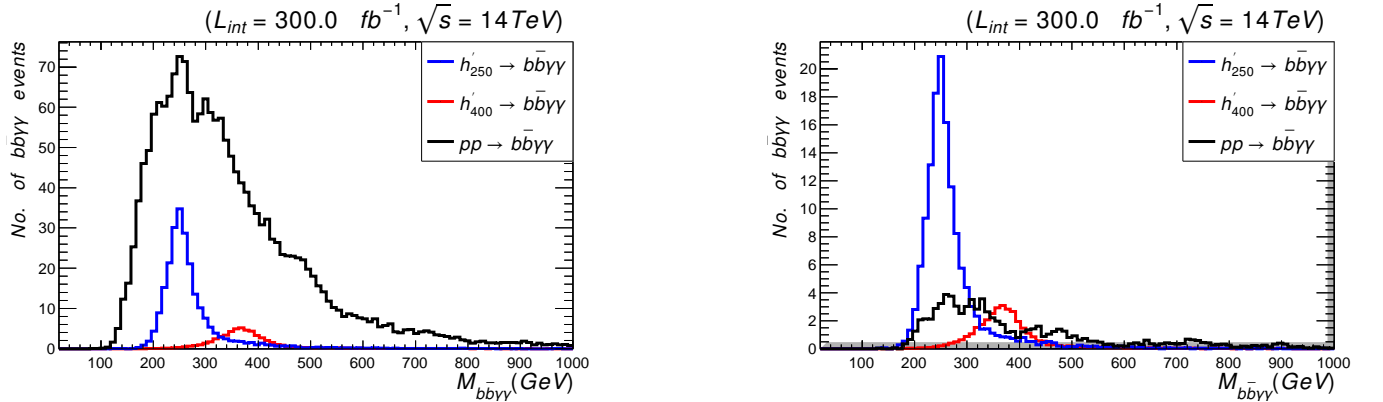


FIG. 5. Number of signal events for $h' \rightarrow b\bar{b}\gamma\gamma$ decays at mass $m_{h'} = 250$ GeV (blue) and 400 GeV (red) induced by ggF versus the invariant mass of the final states $b\bar{b}\gamma\gamma$, at $\sqrt{s} = 14$ TeV and $L_{\text{int}} = 300 \text{ fb}^{-1}$ alongside the relevant background events (black) before (left) and after (right) applying the cut flow of Table V. The corresponding values of cross sections and branching ratios are given in Table IV.

The cut flow in Table V is chosen upon full analysis of final state signal and background kinematics to optimize relative signal-to-background significance (S/\sqrt{B}). As mentioned earlier, for $m_{h'} = 250$ GeV, 400 GeV with $L_{\text{int}} =$

300 fb^{-1} the most relevant cuts were taken around the two SM Higgs peaks in the two photon and two jets invariant mass distributions. Applying these cuts, a major part of the background events were excluded, as it has broad distributions because they were generated as elastic scattering rather than being from resonances at the regions of interest. Eventually, the backgrounds reduced relative to the signals at $m_{h'} = 250 \text{ GeV}$, 400 GeV as in Fig. 5 (right).

From these results, it is clear that the SM-like Higgs boson pair production with $2\gamma + 2b$ -jets can be the smoking gun for probing the heavy CP -even neutral Higgs boson in this class of models that allows for a significant coupling between h' and the SM-like Higgs h boson, unlike several other extensions of the SM. The significance of the $h' \rightarrow b\bar{b}\gamma\gamma$ signal is presented in Fig. 6, for L_{int} values which vary from 100 fb^{-1} up to 3000 fb^{-1} at $\sqrt{s} = 14 \text{ TeV}$, for the usual three values of $m_{h'}$. It is clear that the signal significance increases with considered L_{int} for each value of $m_{h'}$ giving better chances of h' discovery with higher L_{int} .

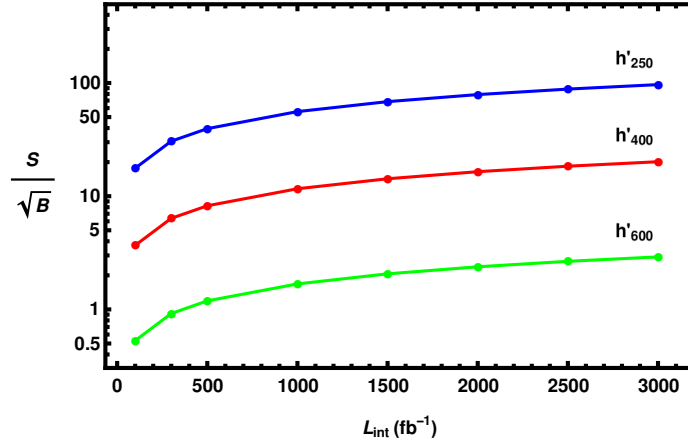


FIG. 6. Significance of the $h' \rightarrow b\bar{b}\gamma\gamma$ signal of Fig. 5 relative to the corresponding background versus L_{int} at mass $m_{h'} = 250 \text{ GeV}$ (blue), 400 GeV (red) and 600 GeV (green). Data are produced at $\sqrt{s} = 14 \text{ TeV}$, and points are interpolated between values of $L_{\text{int}} = 100, 300, 500, 1000, 1500, 2000, 2500 \text{ fb}^{-1}$ and $L_{\text{int}} = 3000 \text{ fb}^{-1}$. Notice that event rates are computed after the cuts described in Table V, and the relative significance of the signals increases with L_{int} .

Cuts (select)	Signal (S): $m_{h'} = 600 \text{ GeV}$	Background (B)	S/\sqrt{B}
Initial (no cut)	155.000	250650.00	0.310
$M_{bb} < 200.0 \text{ GeV}$	52.250 ± 5.18	39823.60 ± 82.40	0.264 ± 0.0008
$M_{\gamma\gamma} > 119.5 \text{ GeV}$	34.436 ± 5.91	4252.00 ± 64.70	0.530 ± 0.0010
$M_{\gamma\gamma} < 130.5 \text{ GeV}$	33.542 ± 5.13	1084.10 ± 32.00	1.018 ± 0.0004
$(\Delta R)_{\gamma\gamma} < 2.0$	29.230 ± 4.35	200.50 ± 17.08	1.062 ± 0.0500
$(\Delta R)_{bb} < 2.0$	27.680 ± 4.46	132.83 ± 7.66	2.409 ± 0.0200
$(P_T)_{\gamma\gamma} > 200.0 \text{ GeV}$	21.650 ± 4.36	57.65 ± 7.70	2.851 ± 0.0260

TABLE VI. Cut flow charts for the $h' \rightarrow hh \rightarrow b\bar{b}\gamma\gamma$ signal versus its relevant background and the corresponding number of events and significance at $L_{\text{int}} = 3000 \text{ fb}^{-1}$ and $\sqrt{s} = 14 \text{ TeV}$ for $m_{h'} = 600 \text{ GeV}$.

With $m_{h'} = 600 \text{ GeV}$, one must consider higher $L_{\text{int}} \sim 3000 \text{ fb}^{-1}$, as the associated production and decay cross section are quite small. Here we apply the cut flow given in Table VI. After applying all these cuts, the final distributions of this event are shown in Fig. 7. According to the plots shown in Fig. 6 and Fig. 7, it is clear that even h' with $m_{h'} \gtrsim 600 \text{ GeV}$ can still be discovered, but at the High-Luminosity Large Hadron Collider (HL-LHC), as it requires L_{int} of order $L_{\text{int}} = 3000 \text{ fb}^{-1}$.

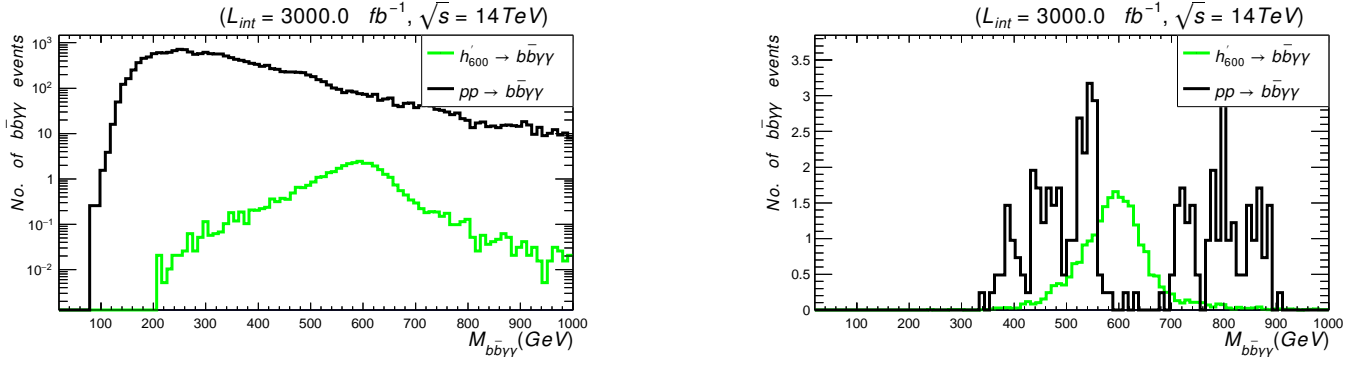


FIG. 7. Number of signal events for $h' \rightarrow b\bar{b}\gamma\gamma$ decays at mass $m_{h'} = 600$ GeV (green) induced by ggF versus the invariant mass of the final states $b\bar{b}\gamma\gamma$, at $\sqrt{s} = 14$ TeV and $L_{\text{int}} = 3000$ fb $^{-1}$ alongside the relevant background events background (black) before (left) and after (right) applying the cut flow set of Table VI. The corresponding values of cross sections and branching ratios are given in Table IV. Left panel is plotted on log-scale vertical axis for the signal to show up relatively.

B. Search for h' Higgs boson in $h' \rightarrow ZZ \rightarrow 4\ell$

Here, we consider the possibility of probing h' through its final decay into four charged leptons, along the process $pp \rightarrow h' \rightarrow ZZ \rightarrow 4\ell$ ($\ell = e, \mu$) with the Feynman diagram in Fig. 8.

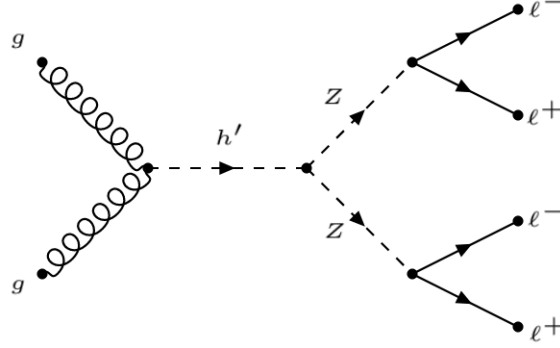


FIG. 8. Feynman diagram for the h' ggF production and decay process $gg \rightarrow h' \rightarrow ZZ \rightarrow 4\ell$.

In the narrow width approximation, the total cross section can be written as

$$\sigma(pp \rightarrow h' \rightarrow ZZ \rightarrow 4\ell) \approx \sigma(pp \rightarrow h') \times \text{BR}(h' \rightarrow ZZ) \times (\text{BR}(Z \rightarrow 2\ell))^2, \quad (52)$$

and the $g_{h'ZZ}$ coupling is given in Eq. (49). As explained below Eq. (49), the $g_{h'ZZ}$ coupling can be as large as $\mathcal{O}(60)$ GeV causing the total cross section $\sigma(pp \rightarrow h' \rightarrow ZZ \rightarrow 4\ell)$ to drop quickly with the propagator mass $m_{h'}$ without any compensation from elsewhere, unlike the previous case of the $h' \rightarrow hh \rightarrow b\bar{b}\gamma\gamma$ due to the propagator mass $m_{h'}$ can be partially compensated for from the coupling $g_{h'hh}$. Therefore, it is rather difficult to detect h' through this channel for heavy h' . In this aspect, we will focus our analysis on $m_{h'} = 250$ GeV. The h' production cross section, its decay branching ratio and the total cross section of $\sigma(pp \rightarrow h' \rightarrow ZZ \rightarrow 4\ell)$ are explicitly shown in Table VII, for $m_{h'} = 250$ GeV and 400 GeV.

It is clear from the results in Table VII that with such small cross sections (fractions of fb), the number of associated events would be extremely smaller than the relevant background, as shown in Fig. 9 (left). Here, we consider larger $L_{\text{int}} = 3000$ fb $^{-1}$ for the both cases of $m_{h'} = 250$ GeV and 400 GeV.

$m_{h'}$ (GeV)	$\sigma(pp \rightarrow h')$ (pb)	$\text{BR}(h' \rightarrow ZZ)$	$\sigma(pp \rightarrow h' \rightarrow ZZ \rightarrow 4\ell)$ (fb)
250	12.140	0.050	0.2428
400	5.050	0.025	0.0579

TABLE VII. $pp \rightarrow h'$ production cross section and its $h' \rightarrow ZZ$ decay branching ratio and the total cross section for its production and decay process $pp \rightarrow h' \rightarrow ZZ \rightarrow 4\ell$ for three different values of $m_{h'} = 250$ GeV and 400 GeV.

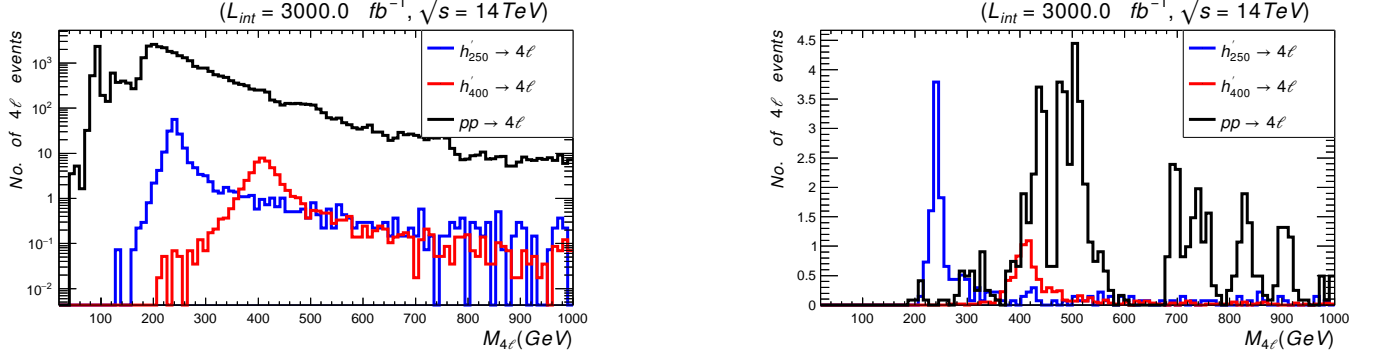


FIG. 9. Number of signal events for $pp \rightarrow h' \rightarrow ZZ \rightarrow 4\ell$ decays at mass $m_{h'} = 250$ GeV (red) and 400 GeV (blue) induced by ggF versus the invariant mass of the final states 4ℓ , at $\sqrt{s} = 14$ TeV and $L_{\text{int}} = 3000 \text{ fb}^{-1}$ alongside the relevant background events background (black) before (left) and after (right) applying the cut flow of Table VIII. The corresponding values of cross sections and branching ratios are given in Table VII.

Again, as our signal is boosted away by the high mass value of the h' Higgs boson, an appropriate cut on the missing transverse hadronic energy $\cancel{E}_T = |-\sum_{\text{jet}} (\vec{P}_T)_{\text{jet}}|$ is applied as emphasized in Table VIII to enhance the relative significance of our signal to the corresponding irreducible background $pp \rightarrow 4\ell$. Accordingly, the background is

Cuts (select)	Signal (S): $m_{h'} = 250$ GeV (400 GeV)	Background (B)	S/\sqrt{B}
Initial (no cut)	728.00 (174.00)	79890.00	2.58000 (0.43000)
$\cancel{E}_T > 150.0$ GeV	58.65 ± 7.34 (38.20 ± 2.01)	247.70 ± 15.70	2.02457 ± 0.00790 (1.26340 ± 0.00597)

TABLE VIII. Cut flow charts for the $h' \rightarrow ZZ \rightarrow 4\ell$ signal versus its relevant background and the corresponding number of events and significance at 3000 fb^{-1} and $\sqrt{s} = 14$ TeV for $m_{h'} = 250$ GeV, 400 GeV.

reduced significantly as shown in Fig. 9 (right). However, the signal is also reduced and only a fraction of events would be available, which indicates that it is not possible to observe this signal via this channel. In Fig. 10, we present the significance of the $pp \rightarrow h' \rightarrow ZZ \rightarrow 4\ell$ signal to the corresponding background versus L_{int} , for mass $m_{h'} = 250$ GeV and 400 GeV, and $\sqrt{s} = 14$ TeV. It is clear from this plot that this signal can not be probed (*i.e.*, $S/\sqrt{B} > 1$), unless we have $L_{\text{int}} \sim 3000 \text{ fb}^{-1}$.

V. CONCLUSIONS

We have proposed a simplified LR model, where $SU(2)_R \times U(1)_{B-L}$ symmetry is broken spontaneously by the VEV of a scalar doublet χ_R around TeV scale, and the electroweak symmetry $SU(2)_L \times U(1)_Y$ is broken by the VEVs of two Higgs doublets merged from a single bidoublet ϕ . We adopted IS mechanism to generate light neutrino masses. We also analyzed the Higgs sector in detail, in particular the three neutral CP -even Higgs bosons. We showed that the lightest of these particle can be assigned to the SM-like Higgs boson, with mass equals to 125 GeV. The next lightest Higgs boson, h' , which is stemmed from the bidoublet neutral component is of order a few hundred GeVs. We studied the LHC potential discovery for h' in this class of models. We performed analysis for searches for h' by looking

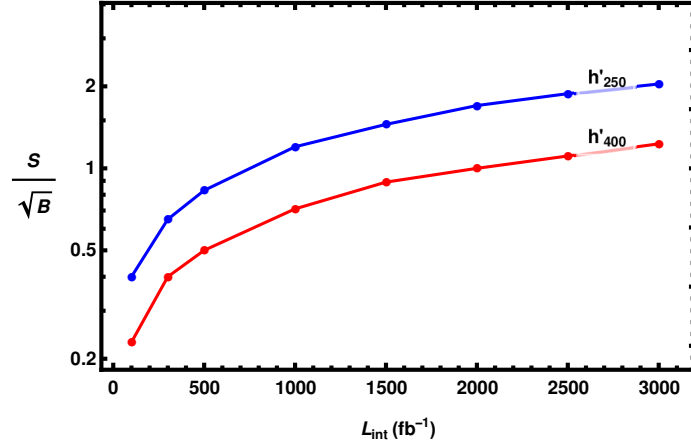


FIG. 10. Significance of the $pp \rightarrow h' \rightarrow ZZ \rightarrow 4\ell$ signal of Fig. 9 relative to the corresponding background versus L_{int} at mass $m_{h'} = 250$ GeV (blue) and 400 GeV (red). Data are produced at $\sqrt{s} = 14$ TeV, and points correspond to $L_{\text{int}} = 100, 300, 500, 1000, 1500, 2000, 2500, 3000 \text{ fb}^{-1}$ and $L_{\text{int}} = 3000 \text{ fb}^{-1}$. Notice that event rates are computed after the cuts described in Table VIII and the relative significance of the signals increases with L_{int} .

for resonant peaks in the following two processes: $h' \rightarrow hh \rightarrow b\bar{b}\gamma\gamma$ and $h' \rightarrow ZZ \rightarrow 4\ell$ ($\ell = e, \mu$). We considered three benchmark points, with $m_{h'} = 250$ GeV, 400 GeV, and 600 GeV, at $\sqrt{s} = 14$ TeV and $L_{\text{int}} = 300 \text{ fb}^{-1}$ and $L_{\text{int}} = 3000 \text{ fb}^{-1}$. We emphasized that h' can be probed with good statistical significances in di-Higgs channel, with $2\gamma + 2b$ -jets final states. While the channel of Z -pair production and decays to 4ℓ is much less significant, it may be observed only at very high $L_{\text{int}} = 3000 \text{ fb}^{-1}$ and for light h' with mass less than 300 GeV.

ACKNOWLEDGEMENTS

M. Ashry and *K. Ezzat* would like to thank *A. Hammad* for the fruitful discussions. This paper is based upon work supported by Science, Technology & Innovation Funding Authority (STDF) under grant number 37272.

VI. APPENDIX

A. TADPOLE EQUATIONS AND POTENTIAL MINIMIZATION

The minimum of the scalar potential (25) is

$$\begin{aligned} \langle V \rangle = V(\langle \phi \rangle, \langle \chi_R \rangle) &= \frac{1}{4} \left[\lambda_1 (k_1^4 + k_2^4) + 4\lambda_4 k_1 k_2 (k_1^2 + k_2^2) + 2(\lambda_1 + 2\lambda_{23}) k_1^2 k_2^2 + 2\mu_1 (k_1^2 + k_2^2) + (\alpha_{13} k_1^2 + \alpha_{12} k_2^2) v_R^2 \right. \\ &\quad \left. + 2k_1 k_2 (4\mu_2 + \alpha_4 v_R^2) + 2\mu_3 v_R^2 + \rho_1 v_R^4 \right], \end{aligned} \quad (53)$$

where the VEVs satisfy the following tadpole equations

$$\frac{\partial \langle V \rangle}{\partial k_1} = \lambda_1 k_1^3 + \lambda_4 k_2 (3k_1^2 + k_2^2) + k_1 \{ k_2^2 (\lambda_1 + 2\lambda_{23}) + \mu_1 + \frac{1}{2} \alpha_{13} v_R^2 \} + 2k_2 \mu_2 + \frac{1}{2} \alpha_4 k_2 v_R^2 = 0, \quad (54)$$

$$\frac{\partial \langle V \rangle}{\partial k_2} = \lambda_1 k_2^3 + \lambda_4 k_1 (k_1^2 + 3k_2^2) + k_2 \{ k_1^2 (\lambda_1 + 2\lambda_{23}) + \mu_1 + \frac{1}{2} \alpha_{12} v_R^2 \} + 2k_1 \mu_2 + \frac{1}{2} \alpha_4 k_1 v_R^2 = 0, \quad (55)$$

$$\frac{\partial \langle V \rangle}{\partial v_R} = \frac{1}{2} v_R \{ \alpha_{13} k_1^2 + 2\alpha_4 k_1 k_2 + \alpha_{12} k_2^2 + 2(\mu_3 + \rho_1 v_R^2) \} = 0. \quad (56)$$

We solve them for μ_1 , μ_2 and μ_3 as follows:

$$\mu_1 = -\lambda_1(k_1^2 + k_2^2) - 2\lambda_4 k_1 k_2 - \frac{\alpha_{12}k_2^2 - \alpha_{13}k_1^2}{2(k_2^2 - k_1^2)} v_R^2, \quad (57)$$

$$\mu_2 = -\frac{1}{2}\lambda_4(k_1^2 + k_2^2) - \lambda_{23}k_1 k_2 - \frac{1}{4}(\alpha_4 + \frac{\alpha_{32}k_1 k_2}{k_2^2 - k_1^2}) v_R^2, \quad (58)$$

$$\mu_3 = -\frac{1}{2}(\alpha_{13}k_1^2 + 2\alpha_4 k_1 k_2 + \alpha_{12}k_2^2 + 2\rho_1 v_R^2). \quad (59)$$

where we define $\alpha_{1i} = \alpha_1 + \alpha_i$, $i = 2, 3$, $\alpha_{32} = \alpha_3 - \alpha_2$ and $\lambda_{23} = 2\lambda_2 + \lambda_3$.

B. COPOSITIVITY CONDITIONS OF THE HIGGS POTENTIAL

To study the boundedness from below and hence, the stability, of the scalar potential (25) we use the copositivity theorems of [51, 52] and follow the procedure used in [14] to ensure that the following symmetric matrix of the quartic terms, which are dominant at higher values of the fields, is copositive:

$$\begin{pmatrix} \lambda_1 & \lambda_1 & \lambda_1 + 2\lambda_{23} & \lambda_1 & \frac{1}{2}\alpha_{13} & \frac{1}{2}\alpha_{12} \\ \cdot & \lambda_1 & \lambda_1 & \lambda_1 + 2\lambda_3 & \frac{1}{2}\alpha_{12} & \frac{1}{2}\alpha_{13} \\ \cdot & \cdot & \lambda_1 & \lambda_1 & \frac{1}{2}\alpha_{12} & \frac{1}{2}\alpha_{13} \\ \cdot & \cdot & \cdot & \lambda_1 & \frac{1}{2}\alpha_{13} & \frac{1}{2}\alpha_{12} \\ \cdot & \cdot & \cdot & \cdot & \rho_1 & \rho_1 \\ \cdot & \cdot & \cdot & \cdot & \cdot & \rho_1 \end{pmatrix}. \quad (60)$$

Copositivity of this matrix demands that $\lambda_1 > 0$, $\rho_1 > 0$, and either of the following cases

1. $\lambda_1 + 2\lambda_{23} > 0$, $\lambda_1 + 2\lambda_3 > 0$, $\alpha_{12} > 0$, $\alpha_{13} > 0$.
2. If $\lambda_1 + 2\lambda_{23} > 0$, $\lambda_1 + 2\lambda_3 < 0$, $\alpha_{12} > 0$, $\alpha_{13} > 0$, then $\lambda_3 < 0$ or $\lambda_1 + \lambda_3 > 0$ and $\lambda_2 > 0$.
3. If $\lambda_1 + 2\lambda_{23} < 0$, $\lambda_1 + 2\lambda_3 > 0$, $\alpha_{12} > 0$, $\alpha_{13} > 0$ then $\lambda_3 < 0$, $\lambda_2 < 0$ and $\lambda_1 + \lambda_{23} > 0$.
4. If $\lambda_1 + 2\lambda_{23} < 0$, $\lambda_1 + 2\lambda_3 < 0$, $\alpha_{12} > 0$, $\alpha_{13} > 0$, then $\lambda_3 < 0$.
5. If $\lambda_1 + 2\lambda_{23} > 0$, $\lambda_1 + 2\lambda_3 > 0$, $\alpha_{12} < 0$, $\alpha_{13} > 0$, then $\lambda_1 \rho_1 > \frac{1}{4}\alpha_{13}^2$ and $\lambda_1 \rho_1 > \frac{1}{2}(\alpha_{12} + \alpha_{13})^2$.
6. If $\lambda_1 + 2\lambda_{23} > 0$, $\lambda_1 + 2\lambda_3 > 0$, $\alpha_{12} > 0$, $\alpha_{13} < 0$, then $\lambda_1 \rho_1 > \frac{1}{4}\alpha_{12}^2$ and $\lambda_1 \rho_1 > \frac{1}{2}(\alpha_{12} + \alpha_{13})^2$.
7. If $\lambda_1 + 2\lambda_{23} > 0$, $\lambda_1 + 2\lambda_3 > 0$, $\alpha_{12} < 0$, $\alpha_{13} < 0$,
then $\lambda_1 \rho_1 > \frac{1}{4}\alpha_{12}^2$ and $\lambda_1 \rho_1 > \frac{1}{4}\alpha_{13}^2$ or $\lambda_1 \rho_1 < \frac{1}{4}\alpha_{12}^2$ and $\lambda_1 \rho_1 < \frac{1}{4}\alpha_{13}^2$.
8. If $\lambda_1 + 2\lambda_{23} < 0$, $\lambda_1 + 2\lambda_3 < 0$, $\alpha_{12} < 0$, $\alpha_{13} < 0$,
then $\lambda_3 < 0$ $\lambda_1 \rho_1 > \frac{1}{4}\alpha_{12}^2$ and $\lambda_1 \rho_1 > \frac{1}{4}\alpha_{13}^2$ or $\lambda_1 \rho_1 < \frac{1}{4}\alpha_{12}^2$ and $\lambda_1 \rho_1 < \frac{1}{4}\alpha_{13}^2$.

Finally, field redefinition could be done to make quartic terms in potential like $\phi_1^0 \phi_2^0 \phi_R^+ \phi_R^-$ nonnegative definite again as in [14].

C. Neutral CP -even Higgs Rotations and Determinant

The explicit rotation coefficients of the CP -even Higgs mass matrix (36) are [53]

$$Z_{11}^H = \frac{f_{11}}{\sqrt{f_{11}^2 + f_{21}^2 + 1}}, \quad (61)$$

$$Z_{12}^H = \frac{f_{21}}{\sqrt{f_{11}^2 + f_{21}^2 + 1}}, \quad (62)$$

$$Z_{13}^H = \frac{1}{\sqrt{f_{11}^2 + f_{21}^2 + 1}}, \quad (63)$$

$$Z_{21}^H = \frac{f_{12}(1 + f_{21}^2) - f_{11}(1 + f_{21}f_{22})}{\sqrt{(1 + f_{11}^2 + f_{21}^2)\{(f_{11} - f_{12})^2 + (f_{21} - f_{22})^2 + (f_{12}f_{21} - f_{11}f_{22})^2\}}}, \quad (64)$$

$$Z_{22}^H = \frac{f_{22}(1 + f_{11}^2) - f_{21}(1 + f_{11}f_{12})}{\sqrt{(1 + f_{11}^2 + f_{21}^2)\{(f_{11} - f_{12})^2 + (f_{21} - f_{22})^2 + (f_{12}f_{21} - f_{11}f_{22})^2\}}}, \quad (65)$$

$$Z_{23}^H = \frac{f_{11}(f_{11} - f_{12}) + f_{21}(f_{21} - f_{22})}{\sqrt{(1 + f_{11}^2 + f_{21}^2)\{(f_{11} - f_{12})^2 + (f_{21} - f_{22})^2 + (f_{12}f_{21} - f_{11}f_{22})^2\}}}, \quad (66)$$

$$Z_{31}^H = \frac{(\text{sgn})(f_{22} - f_{21})}{\sqrt{(f_{11} - f_{12})^2 + (f_{21} - f_{22})^2 + (f_{12}f_{21} - f_{11}f_{22})^2}}, \quad (67)$$

$$Z_{32}^H = \frac{(\text{sgn})(f_{11} - f_{12})}{\sqrt{(f_{11} - f_{12})^2 + (f_{21} - f_{22})^2 + (f_{12}f_{21} - f_{11}f_{22})^2}}, \quad (68)$$

$$Z_{33}^H = \frac{(\text{sgn})(f_{12}f_{21} - f_{11}f_{22})}{\sqrt{(f_{11} - f_{12})^2 + (f_{21} - f_{22})^2 + (f_{12}f_{21} - f_{11}f_{22})^2}}, \quad (69)$$

where the sign term is

$$\text{sgn} = \text{sign}\{f_{11}(f_{23} - f_{22}) + f_{12}(f_{21} - f_{23}) + f_{13}(f_{22} - f_{21})\}, \quad (70)$$

and $f_{ij} = f_i(m_{H_j}^2)$, ($i = 1, 2$, $j = 1 \dots 3$) and the functions f_i 's are

$$f_1(x) = \frac{(m_{22} - x)(m_{33} - x) - m_{23}^2}{m_{12}m_{23} - m_{13}(m_{22} - x)}, \quad (71)$$

$$f_2(x) = -\frac{m_{12}(m_{33} - x) - m_{13}m_{23}}{m_{12}m_{23} - m_{13}(m_{22} - x)}. \quad (72)$$

The determinant of the CP -even Higgs mass matrix (36) is given by

$$\begin{aligned} D^h = & v^2 v_R^2 (-(\alpha_{12}c_\beta + \alpha_4s_\beta)((\alpha_{12}c_\beta + \alpha_4s_\beta)(v^2(c_{2\beta}(\lambda_{23} - \lambda_1) + 2\lambda_4s_{2\beta}) - \frac{1}{4}\alpha_{32}v_R^2sc_{2\beta} + v^2(\lambda_1 + \lambda_{23}) - \frac{\alpha_{32}v_R^2}{4}) \\ & - \frac{1}{4}(\alpha_{13}s_\beta + \alpha_4c_\beta)(4v^2(s_{2\beta}(\lambda_1 + \lambda_{23}) + 2\lambda_4) + \alpha_{32}v_R^2t_{2\beta})) + (\alpha_{13}s_\beta + \alpha_4c_\beta)((\alpha_{12}c_\beta + \alpha_4s_\beta)(v^2s_{2\beta}(\lambda_1 + \lambda_{23}) \\ & + \frac{1}{4}\alpha_{32}v_R^2t_{2\beta} + 2\lambda_4v^2) - (\alpha_{13}s_\beta + \alpha_4c_\beta)(v^2(c_{2\beta}(\lambda_1 - \lambda_{23}) + 2\lambda_4s_{2\beta}) - \frac{1}{4}\alpha_{32}v_R^2sc_{2\beta} + v^2(\lambda_1 + \lambda_{23}) + \frac{\alpha_{32}v_R^2}{4})) \\ & + \rho_1sc_{2\beta}(6v^2c_{2\beta}(\lambda_1\lambda_{23} - \lambda_4^2) + 2v^2c_{6\beta}(\lambda_1\lambda_{23} - \lambda_4^2) + \alpha_{32}\lambda_{23}v_R^2c_{4\beta} - 4\alpha_{32}\lambda_4v_R^2s_{2\beta} - \alpha_{32}v_R^2(2\lambda_1 + \lambda_{23}))). \end{aligned} \quad (73)$$

-
- [1] Y. Fukuda et al. (Super-Kamiokande), Phys. Rev. Lett. **81**, 1562 (1998), hep-ex/9807003.
 [2] M. Ahn et al. (K2K), Phys. Rev. Lett. **90**, 041801 (2003).
 [3] F. An et al. (Daya Bay), Phys. Rev. Lett. **108**, 171803 (2012).
 [4] K. Eguchi et al. (KamLAND), Phys. Rev. Lett. **90**, 021802 (2003).

- [5] Q. Ahmad et al. (SNO), Phys. Rev. Lett. **89**, 011301 (2002).
- [6] R. Mohapatra and J. C. Pati, Phys.Rev. **D11**, 2558 (1975).
- [7] G. Senjanovic and R. N. Mohapatra, Phys.Rev. **D12**, 1502 (1975).
- [8] R. N. Mohapatra, F. E. Paige, and D. Sidhu, Phys.Rev. **D17**, 2462 (1978).
- [9] N. Deshpande, J. Gunion, B. Kayser, and F. I. Olness, Phys.Rev. **D44**, 837 (1991).
- [10] C. S. Aulakh, A. Melfo, and G. Senjanovic, Phys.Rev. **D57**, 4174 (1998).
- [11] A. Maiezza, M. Nemevsek, F. Nesti, and G. Senjanovic, Phys. Rev. D **82**, 055022 (2010).
- [12] D. Borah, S. Patra, and U. Sarkar, Phys.Rev. **D83**, 035007 (2011).
- [13] M. Nemevsek, G. Senjanovic, and V. Tello, Phys.Rev.Lett. **110**, 151802 (2013).
- [14] M. Ashry and S. Khalil, Phys. Rev. D **91**, 015009 (2015), [Addendum: Phys.Rev.D 96, 059901 (2017)].
- [15] R. Mohapatra, Phys. Rev. Lett. **56**, 561 (1986).
- [16] R. Mohapatra and J. Valle, Phys. Rev. D **34**, 1642 (1986).
- [17] M. Gonzalez-Garcia and J. Valle, Phys. Lett. B **216**, 360 (1989).
- [18] C. Weiland, J. Phys. Conf. Ser. **447**, 012037 (2013).
- [19] V. Brdar and A. Y. Smirnov, JHEP **02**, 045 (2019).
- [20] G. 't Hooft, NATO Sci. Ser. B **59**, 135 (1980).
- [21] S. Davidson and H. E. Haber, Phys. Rev. D **72**, 035004 (2005), [Erratum: Phys.Rev.D 72, 099902 (2005)].
- [22] H. E. Haber and D. O'Neil, Phys. Rev. D **83**, 055017 (2011).
- [23] H. E. Haber and D. O'Neil, Phys. Rev. D **74**, 015018 (2006), [Erratum: Phys.Rev.D 74, 059905 (2006)].
- [24] S. Khalil, Phys. Rev. D **82**, 077702 (2010).
- [25] W. Abdallah, A. Awad, S. Khalil, and H. Okada, Eur. Phys. J. C **72**, 2108 (2012).
- [26] G. Aad et al. (ATLAS), Phys. Lett. B **800**, 135082 (2020), 1908.08461.
- [27] G. Senjanović and V. Tello, Phys. Rev. Lett. **114**, 071801 (2015).
- [28] A. Maiezza (2020), 2012.01960.
- [29] L. Wolfenstein, Phys. Rev. Lett. **51**, 1945 (1983), URL <https://link.aps.org/doi/10.1103/PhysRevLett.51.1945>.
- [30] M. Tanabashi et al. (Particle Data Group), Phys. Rev. D **98**, 030001 (2018).
- [31] J. Park (CMS), PoS **ICHEP2018**, 864 (2019).
- [32] A. M. Sirunyan et al. (CMS) (2021), 2102.08198.
- [33] M. Aaboud et al. (ATLAS), JHEP **03**, 174 (2018), [Erratum: JHEP 11, 051 (2018)], 1712.06518.
- [34] M. Frank, O. Özdal, and P. Poulose, Phys. Rev. D **99**, 035001 (2019), 1812.05681.
- [35] G. Aad et al. (ATLAS), Phys. Lett. B **716**, 1 (2012).
- [36] S. Chatrchyan et al. (CMS Collaboration), Phys.Lett. **B716**, 30 (2012).
- [37] P. Bechtle, O. Brein, S. Heinemeyer, O. Stål, T. Stefaniak, G. Weiglein, and K. E. Williams, Eur. Phys. J. C **74**, 2693 (2014).
- [38] P. Bechtle, S. Heinemeyer, O. Stål, T. Stefaniak, and G. Weiglein, Eur. Phys. J. C **74**, 2711 (2014).
- [39] F. Staub, Comput. Phys. Commun. **185**, 1773 (2014).
- [40] W. Porod and F. Staub, Comput. Phys. Commun. **183**, 2458 (2012).
- [41] J. Alwall, M. Herquet, F. Maltoni, O. Mattelaer, and T. Stelzer, JHEP **06**, 128 (2011).
- [42] T. Sjostrand, S. Mrenna, and P. Z. Skands, Comput. Phys. Commun. **178**, 852 (2008).
- [43] J. de Favereau, C. Delaere, P. Demin, A. Giammanco, V. Lemaître, A. Mertens, and M. Selvaggi (DELPHES 3), JHEP **02**, 057 (2014).
- [44] E. Conte, B. Fuks, and G. Serret, Comput. Phys. Commun. **184**, 222 (2013).
- [45] M. Aaboud et al. (ATLAS), JHEP **01**, 030 (2019), 1804.06174.
- [46] A. M. Sirunyan et al. (CMS), JHEP **04**, 112 (2019), 1810.11854.
- [47] A. M. Sirunyan et al. (CMS), JHEP **01**, 054 (2018), 1708.04188.
- [48] G. A. et al, Physics Letters B **801**, 135145 (2020), ISSN 0370-2693.
- [49] J. Chang, K. Cheung, J. S. Lee, C.-T. Lu, and J. Park, Phys. Rev. D **100**, 096001 (2019).
- [50] The-ATLAS-Collaboration (ATLAS), ATLAS NOTE **ATL-PHYS-PUB-2017-001** (2017).
- [51] L. Ping and F. Y. Yu, Linear Algebra and its Applications **194**, 109 (1993), ISSN 0024-3795.
- [52] K. Kannike, Eur.Phys.J. **C72**, 2093 (2012).
- [53] M. Ashry, M.sc. thesis, Cairo University, Cairo (2015).